



# Implementation of an ensemble Kalman filter in the Community Multiscale Air Quality model (CMAQ model v5.1) for data assimilation of ground-level PM<sub>2.5</sub>

Soon-Young Park<sup>1,2</sup>, Uzzal Kumar Dash<sup>1</sup>, Jinhyeok Yu<sup>1</sup>, Keiya Yumimoto<sup>3</sup>, Itsushi Uno<sup>3</sup>, and Chul Han Song<sup>1</sup>

<sup>1</sup>School of Earth Sciences and Environmental Engineering, Gwangju Institute of Science and Technology (GIST), Gwangju, 61005, Republic of Korea

<sup>2</sup>Institute of Environmental Studies, Pusan National University, Busan, 46241, Republic of Korea

<sup>3</sup>Research Institute for Applied Mechanics, Kyushu University, Fukuoka, 816-8580, Japan

**Correspondence:** Chul Han Song (chsong@gist.ac.kr)

Received: 2 September 2021 – Discussion started: 2 November 2021

Revised: 11 February 2022 – Accepted: 2 March 2022 – Published: 6 April 2022

**Abstract.** In this study, we developed a data assimilation (DA) system for chemical transport model (CTM) simulations using an ensemble Kalman filter (EnKF) technique. This DA technique is easy to implement in an existing system without seriously modifying the original CTM and can provide flow-dependent corrections based on error covariance by short-term ensemble propagations. First, the PM<sub>2.5</sub> observations at ground stations were assimilated in this DA system every 6 h over South Korea for the period of the KORUS–AQ campaign from 1 May to 12 June 2016. The DA performances with the EnKF were then compared to a control run (CTR) without DA and a run with three-dimensional variational (3D-Var) DA. Consistent improvements owing to the initial conditions (ICs) assimilated with the EnKF were found in the DA experiments at a 6 h interval compared to the CTR run and to the run with 3D-Var. In addition, we attempted to assimilate the ground observations from China to examine the impacts of improved boundary conditions (BCs) on the PM<sub>2.5</sub> predictability over South Korea. The contributions of the ICs and BCs to improvements in the PM<sub>2.5</sub> predictability were also quantified. For example, the relative reductions in terms of the normalized mean bias (NMB) were found to be approximately 27.2 % for the 6 h reanalysis run. A series of 24 h PM<sub>2.5</sub> predictions were additionally conducted each day at 00:00 UTC with the optimized ICs. The relative reduction of the NMB was 17.3 % for the 24 h prediction run when the updated ICs were applied at 00:00 UTC. This means that after the application of the updated BCs, an

additional 9.0 % reduction in the NMB was achieved for 24 h PM<sub>2.5</sub> predictions in South Korea.

## 1 Introduction

Among many air pollutants, particular attention has been paid to the issue of atmospheric aerosols in East Asia and South Korea, where large anthropogenic emissions from growing economic activities cause frequent episodes of high air pollution. Several environmental and epidemiological studies have suggested that continual exposure to particulate matter with aerodynamic diameter smaller than 2.5 μm (PM<sub>2.5</sub>) has critical effects on human mortality and morbidity (Pope and Dockery, 2006; Cohen et al., 2017; Dehghani et al., 2017). Because of the severity of the influences of PM<sub>2.5</sub> on human health, the accuracy of PM<sub>2.5</sub> forecasts has become a central issue in South Korea. To achieve the goal of improving PM<sub>2.5</sub> predictability, the National Institute of Environmental Research (NIER) of South Korea has implemented daily operational air quality forecast since 2014 using a 3-D chemical transport model (CTM) (Chang et al., 2016), while the Korean Ministry of the Environment (KMoE) provides real-time observations of PM<sub>2.5</sub>, together with the concentrations of five other criteria air pollutants (PM<sub>10</sub>, O<sub>3</sub>, CO, SO<sub>2</sub>, and NO<sub>2</sub>) via a website named “Air Korea” (<https://www.airkorea.or.kr>, last access: 22 March 2022). Although in general the CTM simulation can overcome

the spatial and temporal limitations of ground observations, it has large uncertainties that are due to imperfect emissions, initial conditions (ICs), boundary conditions (BCs), meteorological fields, and physical and photochemical mechanisms (Carmichael et al., 2008; Solazzo et al., 2012).

To improve the accuracy of short-term predictions via CTM simulations, chemical data assimilation (DA) has been proposed as an effective method to reduce the uncertainties in the CTM parameters (e.g., Sandu and Chai, 2011; Zhang et al., 2012a, b; Bocquet et al., 2015; Menut and Bessagnet, 2019). Chemical DA is a technique for integrating information provided by noisy observations and imperfect background estimations from CTM simulations. This integration of the two groups of information can theoretically better represent the true state of the chemical atmosphere. DA techniques have been predominantly applied in the numerical weather prediction (NWP) (Kalnay, 2002), such as optimal interpolation (OI: Lorenc, 1981), the three-dimensional variational method (3D-Var: Lorenc, 1986; Parrish and Derber, 1992; Rabier et al., 1998), the four-dimensional variational method (4D-Var: Talagrand and Courtier, 1987; Courtier et al., 1994; Rabier et al., 2000), and the ensemble Kalman filter (EnKF: Evensen, 2003). While the utilization of DA techniques in air quality predictions has been limited, these techniques have more recently started to be used for air quality prediction as well. To date, several DA methods have been applied to optimize the uncertainties in model input parameters, including ICs (e.g., Elbern and Schmidt, 2001; Park et al., 2016), BCs (e.g., Roustan and Bocquet, 2006), and emission fluxes (e.g., Elbern et al., 2007).

For the past 2 decades, various DA algorithms have been applied, especially to aerosol prediction studies. Several studies have focused on assimilating aerosol observations via OI (Lee et al., 2013; Park et al., 2011, 2014; Tang et al., 2015, 2017; Chai et al., 2017; Lee et al., 2020), 3D-Var (Pagowski et al., 2010; Liu et al., 2011; Schwartz et al., 2012; Saide et al., 2013; Jiang et al., 2013; Li et al., 2013; Pang et al., 2018; Ha et al., 2020), and 4D-Var (Benedetti et al., 2019; Morcrette et al., 2009). All the previous studies mentioned above have reported that the OI, 3D-Var, and 4D-Var assimilations using satellite-retrieved or ground-based observations led to improved aerosol predictability.

Even so, each of these DA methods has its own limitations. OI and 3D-Var usually employ isotropic corrections due to a static (i.e., time-invariant) background error covariance (BEC) based on model climatological profiles. Although 4D-Var has been reported to show better performance than OI and 3D-Var, it requires constant development and maintenance of a tangent linear and adjoint model, which may be a time-consuming and labor-intensive task (Skachko et al., 2014). On the other hand, EnKF is relatively easy to implement without requiring a tangent linear or adjoint model and can easily compute flow-dependent BEC from short-term ensemble predictions. This flow dependence of the BEC is one of the main reasons behind the possible success of the

EnKF method compared to other DA methods. Several studies (Tang et al., 2011; Pagowski and Grell, 2012; Yumimoto and Takemura, 2015; Rubin et al., 2016; Yumimoto et al., 2016; Peng et al., 2017, 2018; Lopez-Restrepo et al., 2020) applied the EnKF DA approach to improve the accuracy of air quality prediction via assimilating surface and/or satellite observations. For example, Yumimoto et al. (2016) applied the EnKF method with satellite-retrieved aerosol observations to evaluate the effectiveness of the DA on dust forecasts and found improved agreement between the predictions and observations. More recently, Peng et al. (2017) reported significant improvements in  $PM_{2.5}$  prediction via the joint optimization of ICs and emissions using the EnKF method by assimilating ground-based  $PM_{2.5}$ .

To optimize the ICs, two studies (Lin et al., 2008; Candiani et al., 2013) carried out assimilation using ground-based aerosol observations with different variants of EnKF DA algorithms. However, few studies have applied the EnKF method to examine the importance of BCs. When long-range transport is an important issue, BCs can provide important information. For example, Constantinescu et al. (2007a) extended the EnKF method to consider lateral BCs and correct emission flux factors in the assimilation process by solving the state parameter estimation problem. Other than this study, no prior study has applied the EnKF method to this type of research, particularly with the Community Multiscale Air Quality (CMAQ) model.

This work is a new endeavor to develop an EnKF DA system for the CMAQ model. The period of the KORUS–AQ campaign 2016 (1 May to 11 June 2016) was chosen to be the target period to test the developed EnKF DA system, since this period includes well-defined and various types of air pollution episodes, e.g., yellow dust events, stagnant high-PM episodes, long-range transport events, and rainy days (Peterson et al., 2019; Jordan et al., 2020). To improve the predictability of  $PM_{2.5}$  in South Korea for this period, ground-based  $PM_{2.5}$  data were assimilated to update the IC and BC fields. Since this is our first attempt to develop an EnKF DA system, we also compared the performances of the EnKF DA system with the existing 3D-Var DA algorithm (Lee et al., 2022).

We believe that this study can be distinguishable from other EnKF studies in three aspects: (i) the EnKF chemical DA system was first developed to assimilate  $PM_{2.5}$  for or with the CMAQ model. In particular, this study intended to enhance the accuracy of  $PM_{2.5}$  prediction via assimilating ground-observed  $PM_{2.5}$  in South Korea (nearly 150 stations) and China (nearly 850 stations). The advantages of the assimilation of ground-observed  $PM_{2.5}$  are also discussed in the text. (ii) The first developed EnKF DA system was applied to  $PM_{2.5}$  predictions in South Korea, where air quality is frequently influenced by long-range transport from the eastern, northern, and northeastern parts of China (EC, NC, and NEC in Fig. 1). (iii) To evaluate the influences of inflow from China on air quality in South Korea more quantitatively,

this study assimilated the ground observations from China and South Korea separately.

The remainder of this paper is organized as follows. Section 2 describes the methodology of this study, including the DA algorithm, CTM, observations, and experimental settings. Section 3.1 discusses the effects of assimilation of ground-based observations and then compares the results with those from 3D-Var based on the reanalysis results. Section 3.2 provides the results of improved BCs in 1d prediction simulations. Section 3.3 quantifies the contributions of updating ICs and BCs with statistical analysis. Finally, Sect. 4 concludes the paper.

## 2 Methods

### 2.1 Ensemble Kalman filter (EnKF)

The EnKF is a DA technique first introduced by Evensen (1994), which was an approximate version of the Kalman filter (KF) (Kalman, 1960). The basic principle of the KF is to estimate a true state, while minimizing the variances of the state with a linear combination of the best estimates of the model and the observations. The optimal state estimated from the KF shows less uncertainty than the model predictions and observations. This optimal state is called the “analysis”. To apply the KF to a nonlinear model, a tangent linear model needs to be constructed, as does its adjoint. However, the EnKF requires neither a tangent linear model nor its adjoint, since it employs Monte Carlo approximation that can estimate the model error covariances using finite ensemble simulations (Evensen, 1994). In particular, the model error covariances used in the EnKF technique are flow-dependent, which is one of the major differences from other DA methods.

The theoretical foundation of the EnKF method proposed by Evensen (2003) is briefly presented below.

$$\mathbf{x}_{i,k}^f = \mathcal{M}\mathbf{x}_{i,k-1}^a + \mathbf{q}_{i,k}, \quad i = 1, 2, \dots, N \quad (1)$$

$$\mathbf{y}_{i,k}^o = \mathbf{y}_k^o + \boldsymbol{\epsilon}_{i,k}^o \quad (2)$$

$$\mathbf{x}_{i,k}^a = \mathbf{x}_{i,k}^f + \mathbf{K}_k \left( \mathbf{y}_{i,k}^o - \mathbf{H}\mathbf{x}_{i,k}^f \right) \quad (3)$$

$$\mathbf{K}_k = \mathbf{P}_k^f \mathbf{H}^T \left( \mathbf{H}\mathbf{P}_k^f \mathbf{H}^T + \mathbf{R}_k \right)^{-1} \quad (4)$$

Here, the subscripts  $i$  and  $k$  represent the  $i$ th ensemble member and the time sequence, respectively. In this set of equations, the first information to estimate the true state is the forecast state  $\mathbf{x}_{i,k}^f$  in Eq. (1). This is the predicted state estimated from the model simulation ( $\mathcal{M}$ ) using the updated initial state,  $\mathbf{x}^a$ , of the previous time step ( $k-1$ ). Here,  $\mathbf{x}_{i,k-1}^a$  is obtained via DA. The model predictions also include pseudo-random model error,  $\mathbf{q}$ , drawn from a Gaussian probability distribution function (PDF) with zero mean value and covariance,  $\mathbf{P}^f$ , [ $\mathbf{q} \sim N(0, \mathbf{P}^f)$ ]. The second piece of information is the observations,  $\mathbf{y}_i^o$ , at time  $k$ , which are randomly sampled

from the PDF of the observations. The PDF of the observations can be generated based on error information from the observed values. Each ensemble member is generated with the assimilation of perturbed observations ( $\mathbf{y}_i^o$ ). The new analyses are then conducted following Eq. (3). These analyses are used for the next ensemble predictions (we term them “propagations”).  $\mathbf{H}$  is a linear operator that transforms the model space into the observation space.  $\mathbf{K}$  is the Kalman gain matrix at a specific time that includes both model and observation errors shown in Eq. (4). The observation error covariance matrix,  $\mathbf{R}$ , contains measurement and representation errors and can be calculated from the defined observation error,  $\boldsymbol{\epsilon}^o$ , [ $\mathbf{R} = \boldsymbol{\epsilon}^o(\boldsymbol{\epsilon}^o)^T$ ].  $\mathbf{P}^f$  is the model error covariance matrix that explains the spatial error correlations and error correlations among the model variables. This can be estimated via the ensemble approach formulated in Eqs. (5) and (6) shown below.

$$\mathbf{P}_k^f \mathbf{H}^T \equiv \frac{1}{N-1} \sum_{i=1}^N \left( \mathbf{x}_{i,k}^f - \overline{\mathbf{x}_k^f} \right) \left( \mathbf{H}\mathbf{x}_{i,k}^f - \overline{\mathbf{H}\mathbf{x}_k^f} \right)^T \quad (5)$$

$$\mathbf{H}\mathbf{P}_k^f \mathbf{H}^T \equiv \frac{1}{N-1} \sum_{i=1}^N \left( \mathbf{H}\mathbf{x}_{i,k}^f - \overline{\mathbf{H}\mathbf{x}_k^f} \right) \left( \mathbf{H}\mathbf{x}_{i,k}^f - \overline{\mathbf{H}\mathbf{x}_k^f} \right)^T \quad (6)$$

The overbar represents the ensemble mean. One of the advantages of the EnKF method is that instead of storing a full covariance matrix ( $\mathbf{P}^f$ ), the error statistics can be computed by Eqs. (5) and (6) using ensembles of model states with the assumption that the ensemble mean can be the best estimate of the true state.

The practical approaches to implement Eqs. (1)–(6) are described as follows. First, through multiple pre-sensitivity tests with the considerations of both model performances and computational costs, the total number of ensembles ( $N$ ) was determined to be 40. Although the results of these sensitivity tests are not presented in this paper, this number of ensemble members ( $N=40$ ) has generally been used in many other EnKF applications (e.g., Schutgens et al., 2010; Coman et al., 2012; Dai et al., 2014).

Second, the diagonal components in the observation error covariance matrix,  $\mathbf{R}$ , were calculated based on the assumption that no errors are correlated among observation locations. The components of  $\mathbf{R}$  matrix have been estimated, while considering the contributions from measurement and representation errors in several previous studies (e.g., Schwartz et al., 2014; Peng et al., 2017; Chen et al., 2019). The application of this method to the observation data resulted in average observation errors of around 5% of the observed values. Therefore, for simplicity, in this study the observation errors were set to be 5% of the observations. To generate perturbed observations ( $\mathbf{y}_{i,k}^o$ ) at a specific time in Eq. (2), 40 random samples ( $\boldsymbol{\epsilon}_i^o$ ) were drawn from the Gaussian distribution having 0 mean value and standard deviations of 5% of the observation values.

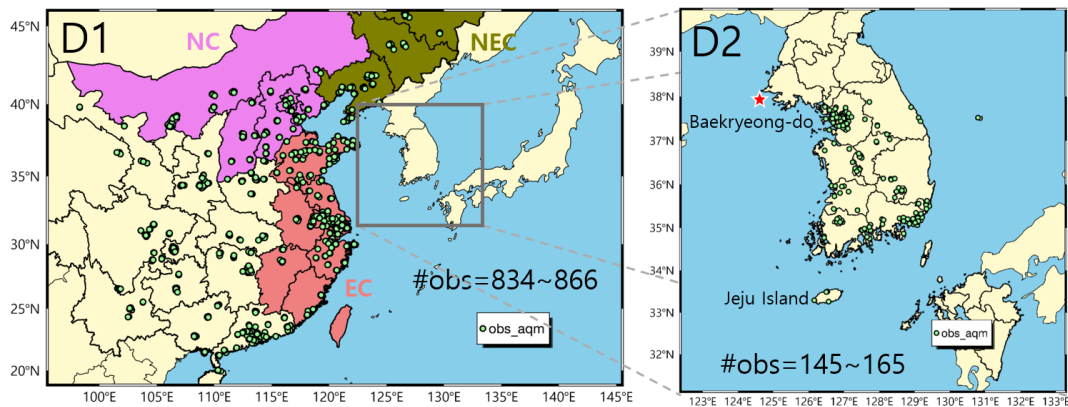


**Figure 1.** Simulation domains with nested modeling. D1 and D2 represent the mother and daughter domain, respectively. The locations of ground stations in China (D1) and South Korea (D2) are marked on the maps with green dots. In D1 (left), the northeastern China (NEC), northern China (NC), and eastern China (EC) regions that frequently influence air quality in South Korea are grouped with olive, violet, and coral colors, respectively. The red star symbol indicates Baekryeong-do observatory, where the evaluation of boundary inflow was made. Jeju Island in D2 (right) is an ideal location to see the flow-dependent correction by the EnKF DA. The total number of available stations used in EnKF data assimilation is also shown in both domains.

Because almost no observation locations exactly match the uniform model grid points, an observation operator,  $\mathbf{H}$ , is required to interpolate the model grid point concentrations to the observation locations. Thus,  $\mathbf{H}$  was constructed in the form of a matrix with weighting factors proportional to the inverse distances from the four edge points of the model grid that surrounds the observation location. Because the CMAQ model does not provide  $\text{PM}_{2.5}$  directly, we calculated the  $\text{PM}_{2.5}$  using a post-processing tool (<https://github.com/USEPA/CMAQ/tree/main/POST/combine>, last access: 22 March 2022) rather than considering all the aerosol species for the  $\mathbf{H}$  matrix. After assimilating the observed  $\text{PM}_{2.5}$ , we applied the increment ratio to all the  $\text{PM}_{2.5}$ -related aerosol species based on the original contributions because the  $\text{PM}_{2.5}$  is a single control variable in this study.

Third, the method to generate the ensemble spread for the model ( $\mathbf{x}_i^f$ ) is as follows: in the CTM runs, the state vector  $\mathbf{x}$  is propagated from time  $k-1$  to time  $k$ . This can be expressed in the following discrete form:

$$\mathbf{x}_i^f(k) = \mathcal{M}(\mathbf{x}_i^b(k-1), \boldsymbol{\eta}_i^b(k-1)). \quad (7)$$

Here, the superscripts  $f$  and  $b$  denote forecast and background, respectively, while  $\mathcal{M}$  denotes the model dynamic operator. The subscript  $k$ , representing time in the previous section, is replaced by  $(k)$  here. The state vector  $\mathbf{x}$  defined in our study represents the  $\text{PM}_{2.5}$  IC to be updated, and  $\boldsymbol{\eta}$  represents the model parameters that are perturbed but not updated through EnKF. This indicates that the multivariate covariances among the aerosol species are not considered. In this study, emissions and BCs were considered to be  $\boldsymbol{\eta}$ . The approaches to generate initial ensembles, emissions, and BCs via random perturbation are described below.

The initial ensembles were created by perturbing the background values of state vector,  $\mathbf{x}^b$ , at time  $t=0$  following the

equation below:

$$\mathbf{x}_i^b(0) = \mathbf{x}^b(0) + \delta\mathbf{x}_i(0), \quad i = 1, 2, \dots, N, \quad (8)$$

where  $\delta\mathbf{x}_i$  represents the  $N$  number of random samples selected from the Gaussian distribution with zero mean and standard deviations of 50% of the background concentration at each corresponding model grid. This magnitude of perturbation was applied to all the layers vertically. Because the  $\text{PM}_{2.5}$  at higher altitudes (e.g., above 2 km) was less than  $5 \mu\text{g m}^{-3}$  on average, there was less chance of vertical error correlation. Following this process, we prepared 40 ensemble members ( $N=40$ ) for the initial ensemble. These 40 ICs propagated over time through the CTM ( $\mathcal{M}$ ) with another perturbed parameter ( $\boldsymbol{\eta}$ ).

For perturbing BCs and emission rates, we took time-correlated noise into account to maintain the temporal evolution of those parameters. In addition, avoiding the rapid fluctuations of perturbations is another reason for the use of time-correlated noise (colored noise). The method of adding colored noise is the same as that described in Tang et al. (2011).

$$\boldsymbol{\eta}_i^b(k) = \boldsymbol{\eta}^b(k) + \delta\boldsymbol{\eta}_i(k) \quad (9)$$

$$\delta\boldsymbol{\eta}_i(k) = \alpha\delta\boldsymbol{\eta}_i(k-1) + \sqrt{1-\alpha^2}\boldsymbol{\sigma}\boldsymbol{\omega}_i(k-1), \quad i = 1, 2, \dots, N \quad (10)$$

$$\alpha = \exp(-1/\tau) \quad (11)$$

Here,  $\boldsymbol{\eta}^b$  is the background emission field or BCs,  $\delta\boldsymbol{\eta}_i$  denotes the random perturbation samples obtained from the previous time step, and  $\alpha$  represents the smoothing coefficient, which is a function of time decorrelation scale ( $\tau$ ), for which we used 24 h.  $\boldsymbol{\omega}_i(k-1)$  is the random sample drawn in the previous time step from the Gaussian distribution with zero mean and a standard deviation of 1. For the standard

deviations ( $\sigma$ ), we used 30 % of the boundary inflow concentrations for PM<sub>2.5</sub> and 50 % of the background emission rates. These perturbation ranges for constructing ensemble spreads were also used in all vertical layers, similar to the perturbation of ICs.

In theory, an ensemble of infinite model states can provide the most realistic estimation of the model error. However, because of the limitations of the computational cost, ensembles with finite sizes are used to provide an approximation to the error covariance matrix. A limited ensemble size causes sampling errors. A small ensemble size may lead to underestimation of the prediction error covariances, which is called “filter divergence” (Houtekamer and Mitchell, 1998), and makes spurious corrections in regions remote from the observation locations, which is called “spurious correlation” (Constantinescu et al., 2007b). To avoid such filter divergence and spurious correlation, we applied covariance inflation and localization. The Gaspari–Cohn piecewise polynomial (Gaspari and Cohn, 1999) with a horizontal width of 100 km and a vertical width of 2 km was used to prevent spurious correlation by localizing the model error covariances. By conducting a sensitivity test, we determined these horizontal and vertical limits, which were small enough to remove the spurious correlation but large enough to encompass the spatial error correlation estimated by ensemble predictions (Eqs. 5 and 6). In addition, the relaxation-to-prior-spread (RTPS) inflation (Whitaker and Hamill, 2012) method was applied against the filter divergence by inflating the ensemble spread before and after the DA. The inflation factor 1.0 was chosen through experimentation, while Pagowski and Grell (2012) applied the inflation factor 1.2 for both meteorological and aerosol variables, and Schwartz et al. (2014) used the inflation factors 1.12 and 1.2 for meteorological variables and aerosol species, respectively. Because we did not perturb any meteorological variables to retain the dynamic balances (i.e., assuming no uncertainty in the meteorological model), the spreads in the predicted (or propagated) ensemble were occasionally less than the observation spread. Therefore, we inflated the ensemble spreads before and after the DA rather than using an inflation factor larger than 1.0. To inflate the predicted ensemble (before DA), we used the spread at the previous analysis time (e.g., 6 h before propagation).

## 2.2 Three-dimensional variational data assimilation (3D-Var)

An analysis state generated by 3D-Var is obtained by minimization of the cost function as follows:

$$J \equiv \frac{1}{2} (\mathbf{x}_k - \mathbf{x}_k^f)^T \mathbf{B}^{-1} (\mathbf{x}_k - \mathbf{x}_k^f) + \frac{1}{2} (\mathbf{H}\mathbf{x}_k - \mathbf{y}_k^o)^T \mathbf{R}_k^{-1} (\mathbf{H}\mathbf{x}_k - \mathbf{y}_k^o). \quad (12)$$

Most of the notations in Eq. (12) are the same as those in Eq. (3), except for the time-invariant (static) BEC matrix,  $\mathbf{B}$ .

The National Centers for Environmental Prediction (NCEP) grid point statistical interpolation (GSI) provides the 3D-Var DA algorithm. Based on the GSI version 3.6 (Shao et al., 2016), Lee et al. (2022) modified it, developing an interface with the CMAQ model. The National Meteorological Centre (NMC) method (Parrish and Derber, 1992) was used to provide the  $\mathbf{B}$  matrix that contains the standard deviations, as well as the vertical and horizontal length scales of the model errors. In the NMC method, the model errors were approximated from a set of differences between the model predictions with different lengths of time window. We used a total of 42 pairs of 12 and 24 h model predictions for the BEC calculations, following the method of Schwartz et al. (2012). Including uncertainty in emissions, Lee et al. (2022) showed that the averaged error standard deviation in the first layer was 8.73  $\mu\text{g m}^{-3}$ , and the horizontal and vertical length scale estimated from the  $\mathbf{B}$  matrix were 119.7 km and 8.7 grids, respectively (refer to Fig. 3 in Lee et al., 2022). The details of the 3D-Var development, including the minimization algorithm, observation operator, and observation error covariances, can be found in Lee et al. (2022).

## 2.3 Numerical models and input data

In this study, the EnKF DA algorithm was developed for the Weather Research and Forecasting (WRF)–CMAQ modeling system. The WRF–CMAQ system was run in offline mode, which means that the CMAQ model runs were performed sequentially after the meteorological fields were generated by the WRF model. This section briefly describes the two numerical models, input fields (e.g., emission and meteorology), simulation domains, and observation data used for the DA.

The WRF version 3.8.1 (Skamarock et al., 2008) with the Advanced Research WRF (ARW) dynamical core was used to produce meteorological fields for the CMAQ model simulations. The ARW dynamical core employs fully compressible and nonhydrostatic Euler equations, together with Arakawa C-grid staggering. In the WRF simulations, the final (FNL) operational global analyses data produced by the NCEP (Saha et al., 2010) were used for the ICs and BCs. Temporal and spatial resolutions of the FNL data are 6 h and 0.25°, respectively. To minimize the uncertainty in the meteorological fields, the ground measurements and vertical radiosonde data were also assimilated with 3 and 6 h intervals, respectively, with the Newtonian relaxation (or nudging) method (Stauffer and Seaman, 1990). The hourly meteorological fields were provided by the WRF model simulations, and they were then converted into CMAQ-ready format via the Meteorology–Chemistry Interface Processor (MCIP v4.3; Otte and Pleim, 2010). Table 1 summarizes the detailed model configurations of the WRF model simulations.

The CMAQ model v5.1 (Byun and Ching, 1999; Byun and Schere, 2006) was used in this study to simulate the atmospheric photochemistries, aerosol dynamics, aerosol thermo-

**Table 1.** WRF model configurations selected in this study.

Parametrization	WRF option
Planetary boundary layer	Yonsei University (YSU) scheme (Hong et al., 2006)
Microphysics	WRF single-moment six-class (WSM6) scheme (Hong and Lim, 2006)
Cumulus parameterization	Grell–Freitas ensemble scheme (Grell and Freitas, 2014)
Land surface model	Noah-MP (Niu et al., 2011; Yang et al., 2011)
Shortwave/longwave options	Rapid Radiative Transfer Model for Global Circulation Models (RRTMG) (Iacono et al., 2008)
Surface layer options	Revised MM5 scheme for Jiménez et al. (2012)

dynamics, and transport of atmospheric species. The CMAQ runs have two domains in accordance with our experimental purposes. The horizontal resolutions of the mother domain (D1) and daughter domain (D2) are 27 and 9 km, respectively, with 15 vertical layers, while the model top is at 20 km. Table 2 lists the CMAQ model configuration.

The mother domain (D1) for the CMAQ model simulations covers northeastern Asia including China, the Korean Peninsula, and Japan, and the daughter domain (D2) nested in the D1 targets South Korea (refer to Fig. 1). With this nesting configuration, we intended to examine how the BCs provided by D1 affect the PM<sub>2.5</sub> predictability in D2. Because the PM<sub>2.5</sub> predictability in South Korea is the focus of this study, most of the experiments were carried out in D2, while model simulations over D1 were used to provide D2 with BCs. Table 3 summarizes the domain descriptions for the WRF and CMAQ model runs.

For another important input field into the CMAQ model simulations, emission data were prepared. KORUS v2.0 emission fields (Jang et al., 2020) were employed for anthropogenic emissions in the two domains. This emission inventory also supported official CTM simulations for the KORUS–AQ field campaign in 2016. To prepare biogenic emissions, the Model of Emissions of Gases and Aerosols from Nature (MEGAN v2.1; Guenther et al., 2006, 2012) was run with MODIS land cover data (Friedl et al., 2010), together with MODIS-derived leaf area index (LAI) (Myneni et al., 2002; Yuan et al., 2011). For the MEGAN runs, the same meteorological fields generated from the WRF model simulations were used. For the considerations of fire emissions, the Fire Inventory from NCAR (FINN) was used (Wiedinmyer et al., 2006, 2011).

The observation data used in the EnKF DA experiments were PM<sub>2.5</sub> data obtained from ground stations located in China and South Korea. We acquired the PM<sub>2.5</sub> data over China from the China urban air quality real-time data release platform (<http://106.37.208.233:20035>, last access: 3 March 2020) managed by the Chinese Ministry of Ecology and Environment, along with another complementary website (<http://www.pm25.in>, last access: 3 March 2020). For the PM<sub>2.5</sub> data over South Korea, the data were downloaded from the National Ambient air quality Monitoring Information System (NAMIS) of Korea (<https://www.airkorea.or.kr>,

last access: 3 March 2020). The maximum available observations for PM<sub>2.5</sub> throughout the period of KORUS–AQ campaign were 866 and 165 in China and South Korea, respectively. Figure 1 shows the locations of those ground stations in D1 and D2.

## 2.4 Experimental setup

For the control run (CTR) without DA, hourly predictions were conducted in D1 by the CMAQ model simulations to generate the BCs for D2. After that, using the BCs we implemented 24 h CMAQ predictions over D2 each day from 25 April to 12 June 2016, with the first 5 d for spin-up and the sixth day for adapting times for the EnKF DA. To provide the meteorological inputs into the CMAQ model runs over D2, the WRF model simulations were initialized each day 12 h before the CMAQ initialization. In this case, the first 12 h simulations were regarded as the spin-up times of the meteorological model. To initialize the next 24 h predictions, the CMAQ model utilized the last hour outputs from the previous 24 h predictions.

The initial ensemble of 40 runs was made based on the CTR output obtained at 00:00 UTC on 30 April by perturbing ICs, as described in Sect. 2.1. The ensemble propagations of the CMAQ model simulations started at 00:00 UTC on 30 April. The DA interval for reanalysis purposes was determined to be 6 h. At the end of the first 6 h prediction (or propagation) of this initial ensemble, the first EnKF DA of PM<sub>2.5</sub> was conducted at 06:00 UTC on 30 April, and the updated initial fields from the EnKF DA are termed the “analysis ensemble” ( $\mathbf{x}_{i,k}^a$ ). These analysis states were again propagated until the next EnKF DA step (12:00 UTC) and were then used as the background state ( $\mathbf{x}_{i,k+1}^f$ ) in the next DA step (Eq. 3). Following this process, the analysis–prediction cycle was repeated in the DA sequences to correct the ICs using the EnKF method. Note that the last DA was carried out at 18:00 UTC on 11 June, and the first three cycles were considered to be an adapting time for EnKF. Consequently, the analysis–prediction outputs acquired from the four time cycles a day are considered to be a reanalysis run (“ANL”) rather than predictions. Meanwhile, 24 h predictions (i.e., 24 h DA interval) were also carried out every day, starting from 00:00 UTC on 1 May to 11 June, with the mean state of the analysis fields ( $\mathbf{x}^a$ ). A total of 42 d predictions are performed for the predic-

**Table 2.** CMAQ model configurations selected in this study.

Parametrization	CMAQ option
Aerosol thermodynamics	AERO6 (Appel et al., 2013)
Gas-phase chemistry	SAPRC07tc (Hutzell et al., 2012)
Chemistry solver	Euler backward iterative (EBI) chemistry solver (Hertel et al., 1993)
Dry deposition	M3DRY (Pleim and Xiu, 2003)
Horizontal advection	Yamo global mass-conserving scheme (Yamartino, 1993)
Vertical advection	Vwrf-piecewise parabolic method (Colella and Woodward, 1984)
Horizontal diffusion	Multiscale (Louis, 1979)
Vertical diffusion	Asymmetric Convective Model version 2 (ACM2; Pleim, 2007a, b)

**Table 3.** Domain descriptions for WRF and CMAQ models.

Model	WRF v3.8.1		CMAQ v5.1	
	D1	D2	D1	D2
Horizontal grids	153 × 114	109 × 109	144 × 105	100 × 100
Grid resolution	27 km	9 km	27 km	9 km
Vertical layers	33 layers (top: 50 hPa)		15 layers* (top: 20 km)	
ICs and BCs	NCEP FNL 0.25° data		Predefined clean profiles	
Target periods	00:00 UTC 1 May 2016–00:00 UTC 12 June 2016			

\* The 15 mid-layer heights correspond to 16, 57, 123, 206, 332, 503, 676, 963, 1468, 2174, 3071, 4119, 5614, 8337, and 13 636 m of altitude above ground level.

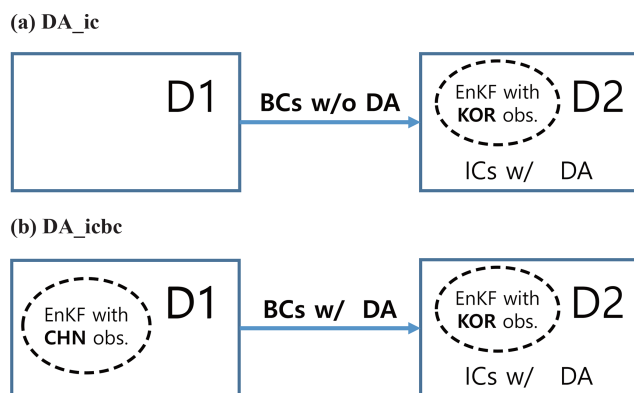


**Figure 2.** Schematic flowchart for the experiments performed in this study. To evaluate  $\text{PM}_{2.5}$  predictability in South Korea, (a) the DA<sub>ic</sub> experiment updates the initial conditions (ICs) only within D2, while (b) the DA<sub>icbc</sub> experiment provides D2 with updated boundary conditions (BCs) via assimilating ground observations in China (CHN obs.) and also updating the ICs for D2 using Korean ground observations (KOR obs.).

tion run (“PRD”) in this study. Figure S1 of the Supplement shows a schematic of these prediction cycles.

In addition to the CTR run, the two experiments labeled DA<sub>ic</sub> (Fig. 2a) and DA<sub>icbc</sub> (Fig. 2b) were also made over South Korea (D2). In both the DA<sub>ic</sub> and DA<sub>icbc</sub> runs, ground-level  $\text{PM}_{2.5}$  collected in D2 was assimilated to update the ICs. The only difference between the two experiments is

the process of acquiring the BCs. In the DA<sub>ic</sub> experiment, the BCs were obtained from the CTR run over D1, while in the DA<sub>icbc</sub> experiment, the BCs were obtained from the runs with the EnKF DA using ground-measured  $\text{PM}_{2.5}$  collected in China. The technical methods to run the ANL and PRD simulations were the same in both the DA<sub>icbc</sub> and DA<sub>ic</sub> experiments.

In the DA<sub>ic</sub> experiment, we updated only ICs, while in the DA<sub>icbc</sub> experiment, we updated both the ICs and the BCs. The goals of this experimental setup are to make it possible to evaluate how much and to what degree the EnKF DA technique could enhance the  $\text{PM}_{2.5}$  prediction skills and to separately estimate the contributions of the improved ICs and BCs to the predictabilities of  $\text{PM}_{2.5}$  over South Korea.

### 3 Results and discussion

#### 3.1 Impact of the improved initial fields

Figure 3 shows the daily variations of surface  $\text{PM}_{2.5}$  from 1 May to 12 June 2016 (KORUS–AQ period). In Fig. 3, the observations (OBS), denoted by open circles, were obtained by averaging all the ground  $\text{PM}_{2.5}$  available in South Korea (we call this the “aggregation plot”). The simulation results (CTR, ANL with the 3D-Var, and ANL with the EnKF) were also calculated by averaging the model outputs at the corresponding observation locations. Figure 3 shows that the control run (CTR) without DA (solid blue line) tended to con-

sistently underestimate the daily averaged  $\text{PM}_{2.5}$  throughout the simulation period. The ANL simulation with the EnKF (solid red line) showed the best agreement with the observations. The performances of the EnKF are also found to be better than those of the 3D-Var (dashed purple line).

Figure 4a and b present the horizontal distributions of surface  $\text{PM}_{2.5}$  for the background and analysis fields at a specific EnKF DA sequence, respectively. Here, the “analysis field” indicates the ICs updated by the EnKF method. Figure 4a and b also plot the observed  $\text{PM}_{2.5}$  used in the DA with the same color scale. Figure 4c gives the analysis increments representing the extent of the corrections of  $\text{PM}_{2.5}$  by the EnKF data assimilation. Again, the background fields tended to underestimate the  $\text{PM}_{2.5}$  over the inland areas. As discussed in Sect. 2.4, Fig. 4b was obtained using an average of 40 analysis ensembles. It can be seen how the estimated background error covariance with a short-term ensemble propagation could correct the model background by assimilating observations. At a relatively isolated ground station, such as Jeju Island (the location is shown in Fig. 1), the analysis increments occurred largely in the downwind area (Fig. 4c). This provides a clear example of flow-dependent correction of the EnKF technique. As another example for clearly showing flow-dependent behavior, the increment comparison between 3D-Var and EnKF is presented in Fig. S2 of the Supplement.

Figure 5 presents the average diurnal variations generated by aggregating the  $\text{PM}_{2.5}$  data during 42 d from all the observation sites. The vertical bars indicate 1 standard deviation of the averaged samples. Figure 5 shows a clear pattern of the results from each simulation, showing distinct diurnal variations. This pattern appears to be caused mainly by the changes in meteorological fields during the day. During daytime, relatively high mixing height due to the thermal and mechanical development of boundary layers could lead to decreased  $\text{PM}_{2.5}$  within the boundary layers. In contrast, after sunset,  $\text{PM}_{2.5}$  started to increase because the mixing height became shallow due to the stable atmospheric conditions caused by sunset and the weak wind speeds. This diurnal pattern was also found in the observation data, but their variations are weaker than those from the model simulations. The CTR experiment again consistently underestimated the diurnal  $\text{PM}_{2.5}$  throughout a day. However, quite good agreement with the observed  $\text{PM}_{2.5}$  was found in the ANL simulations with the EnKF (solid red line). Focusing on the mean values only at each DA time (00:00, 06:00, 12:00, and 18:00 UTC), the updated concentrations for the 3D-Var simulations (purple triangles) are always closer to the observations than those for the EnKF simulations (red triangles). This indicates that the 3D-Var used larger model errors with higher uncertainties than those of the EnKF when the DA process was carried out. However, the EnKF showed better performance than the 3D-Var simulations in the following time, especially during the daytime (e.g., 01:00 to 06:00 UTC and 07:00 to 12:00 UTC), although its correction strength by assimilation

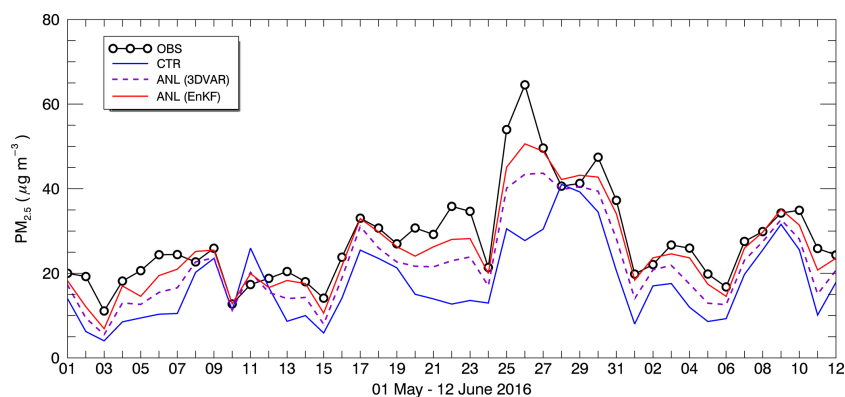
is lower than the 3D-Var. We believe this is because the flow-dependent characteristics of model errors in the EnKF technique improve the model fields more realistically than those in 3D-Var. In contrast, 3D-Var uses a “static” climatological BEC, which usually represents a semi-Gaussian distribution. The better results from the EnKF method (than the 3D-Var method) can also be attributed to the realistic considerations of vertical mixing within the boundary layer in the BEC (Pagowski and Grell, 2012). More sophisticated comparisons in the configurations, such as error variances, observation operator, and vertical length scale of the BEC, are necessary in future study for a direct comparison of the two DA algorithms. To more quantitatively evaluate the performances of the 3D-Var and EnKF techniques, Table 4 also summarizes the statistical metrics based on the reanalysis outputs (ANL). Section 3.4 below discusses the quantitative evaluation in more detail.

### 3.2 Impact of the improved boundary conditions

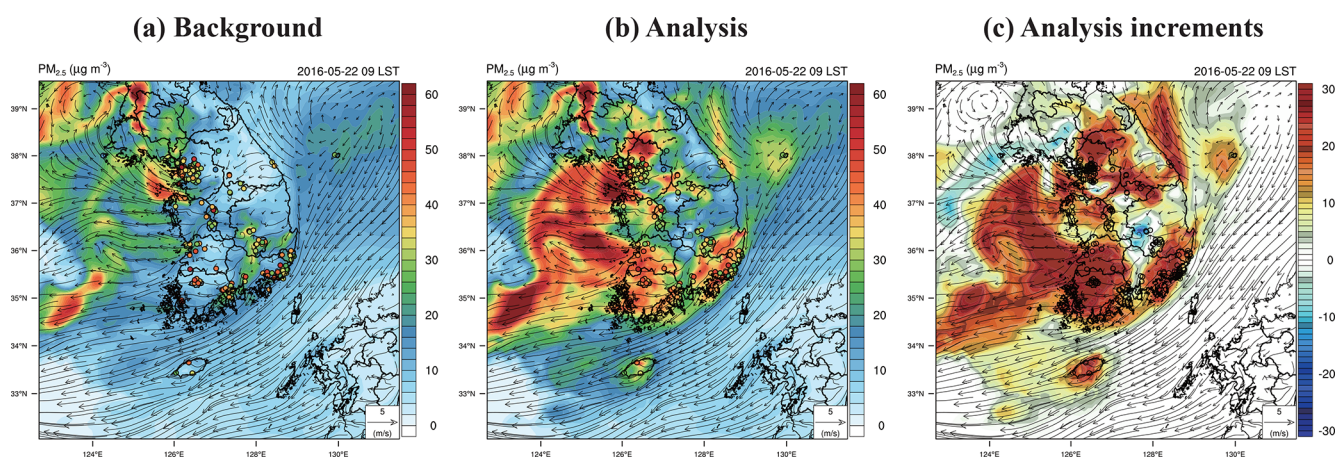
In the previous section, we examined the effects of the initial fields (the DA\_ic experiment) in South Korea. The influences of the updated ICs tend to quickly disappear with time over the relatively small domain (D2), particularly when atmospheric flows are fast. In this section, we conducted additional assimilation with the ground observations from China in D1, in addition to the data assimilation with ground observations from South Korea (the DA\_icbc experiment). The DA\_ic and DA\_icbc experimental results were again compared in South Korea, which is our main domain of interest. Although the prediction strategy (refer to Fig. S1 of the Supplement) was the same in the DA\_icbc experiment, only PRD runs are shown in this section for simplicity.

Figure 6 shows the averaged  $\text{PM}_{2.5}$  used for the four lateral boundaries of domain 2 in both the DA\_ic and DA\_icbc experiments. At the four lateral boundaries,  $\text{PM}_{2.5}$  was averaged over 6 weeks, and Fig. S3 of the Supplement shows the south, east, north, and west boundaries of domain 2 (D2). The color-filled contours on the vertical planes correspond to the longitudinal direction from west to east (latitudinal direction from south to north) and the vertical direction for the southern and northern (western and eastern) boundaries of domain 2. Together with the  $\text{PM}_{2.5}$ , Fig. 6 also plots the mean wind velocity across the four boundaries to show the inflow into D2 and outflow from D2 with positive (solid) and negative (dashed) contour lines, respectively. In the upper panels of Fig. 6, the western part of the north boundary and northern part of the west boundary show relatively high  $\text{PM}_{2.5}$  ( $>15 \mu\text{g m}^{-3}$ ) within 1 km of altitude. Although long-range transport of air pollutants from China to South Korea sometimes occurs in the upper layers, the averaged  $\text{PM}_{2.5}$  at the northwest boundaries were high within the boundary layer. We should also note in Fig. 6 that the northwestern boundary had a strong inflow that could result in high  $\text{PM}_{2.5}$  in D2.





**Figure 3.** Daily variations of surface  $\text{PM}_{2.5}$  for the DA<sub>ic</sub> experiment. Observations (OBS) are represented by a black solid line with open circles. Model results for the control (CTR) run without DA, the reanalysis (ANL) run with 3D-Var, and reanalysis ANL with EnKF are plotted with a blue solid line, purple dashed line, and red solid line, respectively. Values were prepared from daily averages at all the observation sites in South Korea (D2).



**Figure 4.** Snapshots of the horizontal distributions of  $\text{PM}_{2.5}$  before (a) background and after (b) analysis the application of the EnKF technique at 00:00 UTC on 22 May 2016. The observed concentrations are also shown on the map with the same color scales as contour values. In the right-hand panel (c), the analysis increments are also presented, and flow-dependent corrections are visible when the wind vectors are overlaid with the analysis increments. The big island in the Southern Sea of the Korean Peninsula is Jeju Island, where the flow-dependent behavior can be noticed.

The middle and bottom panels of Fig. 6 show that at all the boundaries, the DA<sub>icbc</sub> experiment exhibited higher  $\text{PM}_{2.5}$  than the DA<sub>ic</sub> experiment. This indicates that the control simulation without assimilation (CTR) over D1 under-calculated  $\text{PM}_{2.5}$  in China. Figure 6c shows that there are small changes in  $\text{PM}_{2.5}$  above 2 km of altitude, while the changes become larger within the boundary layers. To quantify the amounts transported into and out of D2, we calculated the  $\text{PM}_{2.5}$  fluxes by multiplying  $\text{PM}_{2.5}$  by wind velocities and then averaged them over the simulation period (refer to Fig. S4 of the Supplement). The cross-sectionally averaged  $\text{PM}_{2.5}$  flux at the west boundary increased from  $19.2$  to  $26.6 \mu\text{g m}^{-2} \text{s}^{-1}$  from the DA<sub>ic</sub> to DA<sub>icbc</sub> experiments. This indicates that larger amounts of  $\text{PM}_{2.5}$  were actually transported long distances from China to South Korea,

mainly through the northwestern boundary of domain 2 during the KORUS–AQ period.

A ground station where the influence of the BCs can be checked is Baekryeong-do, South Korea (shown with a star symbol in Fig. 1). This is because Baekryeong-do is located at the west end of domain 2 (nearly the western boundary of D2) and is also minimally affected by local inland emissions (i.e., there are no major industries and only a small population living on the island). Figure 7a shows the averaged diurnal variations of  $\text{PM}_{2.5}$  at Baekryeong-do evaluated from D1. Hence, the results with (solid red line with triangles) and without (blue dashed line with rectangles) the DA can be perceived as the BCs in D2 for the DA<sub>icbc</sub> and DA<sub>ic</sub> experiments (refer to Fig. 2), respectively. The averaged diurnal variation of  $\text{PM}_{2.5}$  without the DA is in the range between

**Table 4.** Statistical metrics for the experiments of DA\_ic and DA\_icbc. Experiments were evaluated for the 6-hourly assimilated analysis run (ANL) and for the 1 d prediction run (PRD). The ANL run using 3D-Var in the DA\_ic experiment is included for comparison.

Experiments and simulations		MEAN* ( $\mu\text{g m}^{-3}$ )	<i>R</i>	IOA	RMSE ( $\mu\text{g m}^{-3}$ )	MB ( $\mu\text{g m}^{-3}$ )	NMB (%)
CTR		17.9	0.421	0.610	20.8	−10.2	−36.2
DA_ic	ANL (3D-Var)	22.1	0.618	0.761	15.6	−5.8	−20.8
	ANL	25.4	0.646	0.795	14.3	−2.5	−9.0
	PRD	22.9	0.464	0.665	18.8	−5.3	−18.9
DA_icbc	ANL	26.5	0.656	0.804	14.1	−1.4	−5.1
	PRD	25.5	0.484	0.685	18.3	−2.5	−9.9

\* Mean concentration in observed data is  $27.9 \mu\text{g m}^{-3}$ .

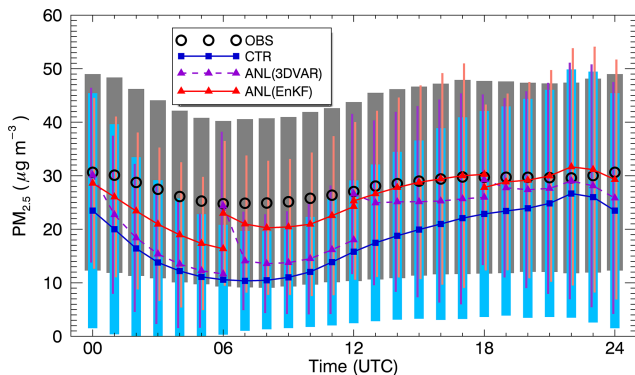


**Figure 5.** Average diurnal variations of  $\text{PM}_{2.5}$  aggregated from all ground stations in South Korea (D2) for the DA\_ic experiment. The color labels are the same as in Fig. 1, except for symbols. The error bars with gray, cyan, purple, and pink indicate 1 standard deviation ( $\pm\sigma$ ) for OBS, CTR, ANL by 3D-Var, and ANL by EnKF simulations, respectively.

10 and  $20 \mu\text{g m}^{-3}$ , which is approximately  $10 \mu\text{g m}^{-3}$  lower than the observed  $\text{PM}_{2.5}$ . However, when the assimilation of the observations in China was applied, almost the same levels of  $\text{PM}_{2.5}$  as the observations were reproduced. We found that the 24 h predictions that were evaluated at the same location in D2 were greatly improved (Fig. 7b). This is confirmed by the results from the DA\_icbc experiment in Fig. 7b. Since the observed  $\text{PM}_{2.5}$  at the Baekryeong-do site was assimilated to improve the ICs in both the DA\_ic and DA\_icbc experiments, the predictions started from a similar  $\text{PM}_{2.5}$  as the observed  $\text{PM}_{2.5}$ . However, the predictions for the DA\_icbc experiment agreed greatly with the observed  $\text{PM}_{2.5}$  owing to the application of accurate BCs, while the prediction for the DA\_ic experiment rapidly converged to the CTR run because of the same BCs as the CTR run. It should also be noted that analysis increments by assimilating Baekryeong-do data for the DA\_icbc experiment in D2 would be minimal, as the background  $\text{PM}_{2.5}$  was already close to the observed  $\text{PM}_{2.5}$  because of the updated BCs.

Figure 8 presents the daily variations of  $\text{PM}_{2.5}$  like in Fig. 3, except for the results from the “PRD runs” for the DA\_ic and DA\_icbc experiments. The PRD runs are technically the same as the ANL runs except for the prediction lead time (of 24 and 6 h, respectively). Again, significant improvements in the DA\_ic and DA\_icbc experiments were found compared to the results from the CTR run. When the dominant synoptic wind directions were southerly or easterly (e.g., on 2 to 4 June), there were only small differences between the DA\_icbc and DA\_ic experiment, and thus limited improvements were achieved. Similarly, no improvements were found during the precipitation days on 10 and 24 May and on 1 and 6 June. However, large improvements could be made when the yellow dust event occurred from 4 to 7 May and when the westerly winds prevailed over D2 between 20 and 27 May (except on 24 May). An example of the impact of the updated BCs for the DA\_icbc experiment is shown in Fig. S5 of the Supplement, which explains the higher transboundary  $\text{PM}_{2.5}$  after assimilating ground  $\text{PM}_{2.5}$  observations in China. Therefore, to improve the predictability of  $\text{PM}_{2.5}$  in South Korea, it is of great importance to provide appropriate BCs by assimilating the ground observation data in the upwind area (i.e., EC, NC, and NEC region, refer to Fig. 1).

To evaluate the  $\text{PM}_{2.5}$  predictability in South Korea, Fig. 9 also displays the averaged diurnal variations and compares the prediction runs (PRD) for the two experiments, DA\_ic and DA\_icbc. The performances of 24 h predictions were launched every 00:00 UTC. The predicted  $\text{PM}_{2.5}$  for the PRD runs shows better performances than the CTR run with reduced errors and biases, although the biases are larger than those for the ANL runs (shown in Fig. 3). Again, the averaged diurnal  $\text{PM}_{2.5}$  for the DA\_icbc experiment is closer to the observations than that for the DA\_ic experiment. This is because the enhanced boundary information was repeatedly provided at the everyday prediction sequence. Also, the negative biases found in the DA\_ic experiment were greatly alleviated with the DA\_icbc experiment, even if the same emissions and meteorological fields were applied for the 24 h

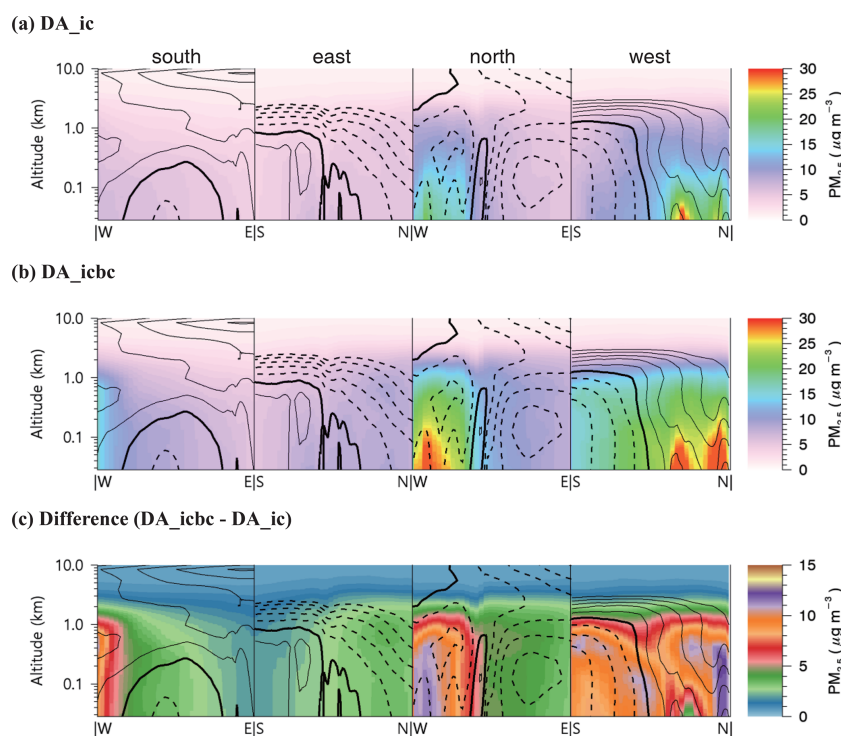


**Figure 6.** Averaged  $\text{PM}_{2.5}$  distributions in the four lateral boundaries of the domain 2 (D2: south, east, north, and west from the left to the right, refer to Fig. S4 of the Supplement). Each panel includes black contour lines that explain the inflow (solid lines) and outflow (dashed lines) wind vector with  $1 \text{ m s}^{-1}$  intervals. The thick black lines indicate zero wind speed. In (a) DA\_ic and (b) DA\_icbc, the averaged lateral boundary conditions are provided into D2 without and with the EnKF data assimilation in China (D1), respectively. The increments in DA\_icbc experiment are also presented in the bottom panel (c). Note that the y axis for altitude is presented in log scale to emphasize the results below the boundary layer.

predictions. Immediate improvements could be seen after the predictions started at 00:00 UTC. As time progressed, the biases and errors were also propagated. However, the biases in the DA\_icbc experiment became about half of those in the DA\_ic experiment. Also note that the slightly overpredicted  $\text{PM}_{2.5}$  for the DA\_icbc experiment between 18:00 and 23:00 UTC was caused by insufficient information about vertical mixing during nighttime. Simulated nocturnal boundary layer heights were lower than real boundary layer heights. This is a critical problem in meteorological modeling and has been discussed in many previous publications (Eder et al., 2006; Hong, 2010).

### 3.3 Statistical evaluations: quantification of contributions by updating the initial and boundary conditions

Table 4 summarizes the statistical performance metrics that were calculated to evaluate the model performance. Table S1 of the Supplement provides the mathematical definitions for the performance metrics. Because the evaluations were conducted using hourly data, including the prediction hours, we did not consider a spatially independent observation. Moreover, it is difficult to randomly select sparse observation sites

(D2 in Fig. 2). Therefore, the statistical metrics were calculated including the same observation data as those used in DA and were compared under the same conditions for all the experiments. The average  $\text{PM}_{2.5}$  over the entire simulation period was  $27.9 \mu\text{g m}^{-3}$ , and the CTR run produced an underestimated  $\text{PM}_{2.5}$  of  $17.9 \mu\text{g m}^{-3}$ . The application of the updated ICs (the DA\_ic experiment) improved the average  $\text{PM}_{2.5}$ , which was  $25.4$  and  $22.9 \mu\text{g m}^{-3}$  for the ANL and PRD runs, respectively. The results for the DA\_icbc experiment were even closer to the observations than those of the DA\_ic. The average  $\text{PM}_{2.5}$  from the ANL and PRD runs for the DA\_icbc experiment was  $26.5$  and  $25.5 \mu\text{g m}^{-3}$ , respectively. All the statistical metrics for the DA\_icbc experiment were improved compared to the DA\_ic experiment. Focusing on the PRD runs, the IOA increased significantly from 0.610 to 0.665 (for the DA\_ic experiment) and then to 0.685 (for the DA\_icbc experiment). The root mean square error (RMSE) was reduced from  $20.8$  to  $18.3 \mu\text{g m}^{-3}$  for the DA\_icbc experiment, while it was  $18.8 \mu\text{g m}^{-3}$  for the DA\_ic experiment. This small reduction in the averaged RMSE between the DA\_ic and the DA\_icbc experiments can be attributed to the overprediction of  $\text{PM}_{2.5}$  during the nighttime, as Fig. 9 shows. On the other hand, remarkable improvements were found in the MBs. In the DA\_ic experiment,

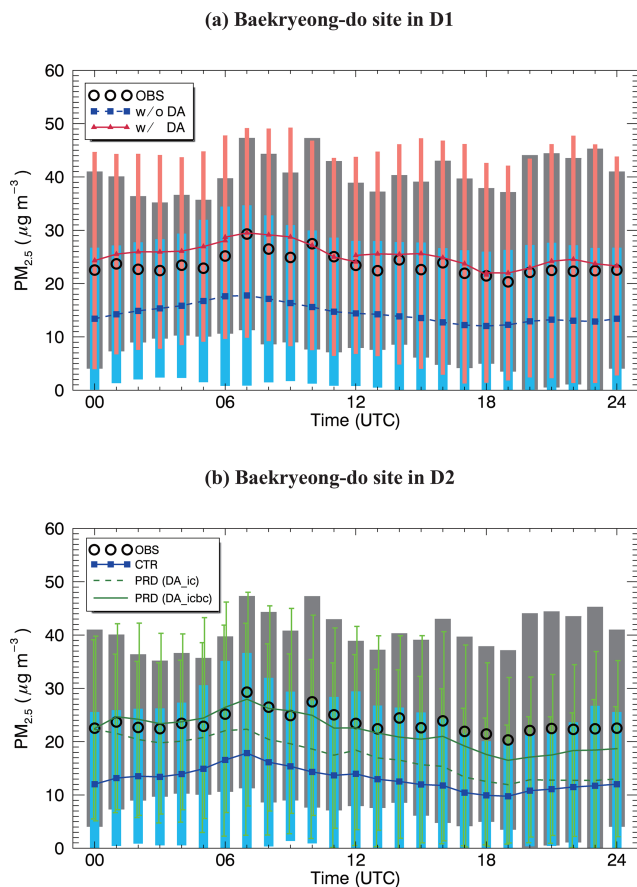


**Figure 7.** Averaged diurnal variations of  $\text{PM}_{2.5}$  aggregated at the Baekryeong-do site from the results obtained in (a) D1 and (b) D2. The line colors and symbols are the same as in Fig. 5, except for the prediction runs in D2, which are plotted by dashed and solid green lines for the DA<sub>ic</sub> and DA<sub>icbc</sub> experiments, respectively, in panel (b).

the averaged MB was drastically reduced from  $-10.2$  to  $-5.3 \mu\text{g m}^{-3}$ . Another large reduction in the averaged MB was found from  $-5.3$  to  $-2.5 \mu\text{g m}^{-3}$  from the DA<sub>ic</sub> experiment to the DA<sub>icbc</sub> experiment. The normalized MB (NMB) was also reduced by 17.3 % in the DA<sub>ic</sub> experiment from 36.2 % for the CTR run. In addition, the DA<sub>icbc</sub> experiment led to another considerable decrease in the NMB by 9.0 % compared to the DA<sub>ic</sub> experiment.

To investigate the quantitative contributions of the ICs and BCs to the model performance, we calculated the “rate of improvement (ROI)” with respect to the PRD results (see Table 5). The ROIs are defined by the ratios of enhanced ( $R$  and IOA) or reduced (RMSE and MB) corresponding statistical metrics to those calculated from the CTR run. Based on the ROI for the DA<sub>ic</sub> and DA<sub>icbc</sub> experiments, we can estimate the ROIs associated with the initial correction (the DA<sub>ic</sub>) and the boundary correction (the DA<sub>bc</sub>). The ROIs for the DA<sub>ic</sub> and DA<sub>icbc</sub> experiments were 10.2 % and 15.0 % in terms of  $R$  (Pearson’s correlation coefficient), re-

spectively. Therefore, the estimated ROI due to the DA<sub>bc</sub> might be 4.8 %. The contributions in MB can also be estimated quantitatively in terms of the ROIs. Updated BCs resulted in an improvement of 27 % in the MB in terms of ROI. In the case of the applications of the DA<sub>ic</sub> and the DA<sub>bc</sub>, the ROIs showed a 9.0 and 3.3 % increase in terms of IOA and a 9.6 % and 2.4 % decrease in terms of RMSE, respectively.

## 4 Conclusions

To improve  $\text{PM}_{2.5}$  prediction in South Korea, we developed and applied an EnKF data assimilation method to the WRF–CMAQ modeling system. For data assimilation, we employed two groups of ground observations from China and South Korea. We found that when we updated the ICs via the EnKF data assimilation, the  $\text{PM}_{2.5}$  predictions in South Korea could be greatly improved. In a comparative analysis between EnKF and 3D-Var, the EnKF technique showed better performance than 3D-Var in short-term  $\text{PM}_{2.5}$  predictions. These results indicate that the BEC used in this study can realistically reflect the current state of the atmosphere, particularly in the boundary layer.

This study also highlighted the importance of updating BCs to further enhance the  $\text{PM}_{2.5}$  predictability over South Korea. Long-range transport from China directly impacts the air quality in South Korea, particularly during high- $\text{PM}_{2.5}$  episodes. Because effects to implement DA with ground observations inside South Korea are restrictive in terms of improvement in analysis fields and predictions, we updated the inflow BCs via the EnKF DA that uses observations in China. A comparison of the studies with and without the updated BCs suggested that improved ICs (the DA<sub>ic</sub> experiment) reduced the NMBs from  $-36.2$  to  $-18.9$  % compared to the control run, and even further updating the ICs and BCs (the DA<sub>icbc</sub> experiment) improved the NMBs from  $-36.2$  to  $-9.9$  % in terms of the 24 h  $\text{PM}_{2.5}$  prediction over South Korea. In terms of IOA (in terms of MB), the contributions of updating the ICs and BCs to 24 h predictability were estimated to be 73 and 27 % (63 and 37 %), respectively. However, caution should be exercised in that these estimations are made only for a specific period (KORUS–AQ campaign) and can vary with atmospheric conditions. A longer test period is needed for general quantification.

Recently, the EnKF has also been used to assimilate satellite-retrieved aerosol observations (e.g., Sekiyama et al., 2010; and Yin et al., 2016). Other groups also used the EnKF method for the joint optimization of ICs and emission scaling factors (e.g., Tang et al., 2011; Peng et al., 2017 and 2018). As we have shown that the consideration of transboundary air pollution is of significance in the  $\text{PM}_{2.5}$  predictions over South Korea, assimilating aerosol optical depth (AOD) data from satellites over the Yellow Sea (where no ground obser-

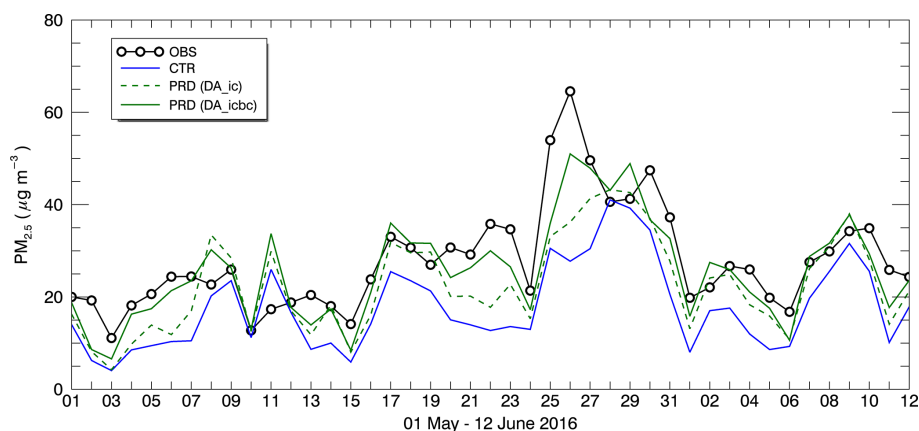


**Figure 8.** Daily averaged variations of  $\text{PM}_{2.5}$ . The lines and colors are the same as in Fig. 3, except for the 1 d prediction runs (PRD). The 1 d predictions only with updated initial conditions (DA\_ic) and with initial and boundary conditions (DA\_icbc) are presented by the dashed and solid green lines, respectively.

**Table 5.** Rate of improvement (ROI) by EnKF data assimilation in 1 d predictions. The ROI is the ratio of the enhanced ( $R$  and IOA) or reduced (RMSE and MB) statistical metrics to those for the CTR simulation. The ROI by updating boundary conditions (DA\_bc) can be estimated from the difference between that obtained by the DA\_ic and DA\_icbc experiments.

	DA_ic	DA_icbc	Estimated DA_bc
$R$	10.2 %	15.0 %	4.8 %
IOA	9.0 %	12.3 %	3.3 %
RMSE	9.6 %	12.0 %	2.4 %
MB	48 %	75 %	27 %

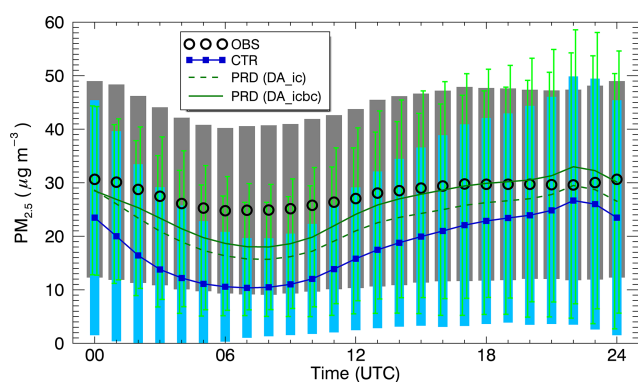


**Figure 9.** Averaged diurnal variations of  $\text{PM}_{2.5}$  aggregated from all ground stations in South Korea (D2). The color and symbols are the same for observations (OBS) and the control run (CTR) as in Fig. 5. The 1 d predictions only with updated initial conditions (DA\_ic) and with initial and boundary conditions (DA\_icbc) are presented by dashed and solid green lines, respectively. 1 standard deviation ( $\sigma$ ) is also plotted for each case using vertical bars. The left and right vertical bars indicate  $\pm\sigma$  for DA\_ic and DA\_icbc, respectively.

vations are available) is expected to provide the  $\text{PM}_{2.5}$  prediction system with important information.

Throughout this study, the DA method of “perturbed observation EnKF” (first proposed by Evensen, 2003) was employed. However, there are some popular variants of the EnKF method that obviate the need to perturb observations, such as the ensemble square root filter (EnSRF; Whitaker and Hamill, 2002), ensemble adjustment Kalman filter (EAKF; Anderson, 2001), and local ensemble transform Kalman filter (LETKF; Hunt et al., 2007). Two of these EnKF variants are also being tested to alleviate the sampling errors in the observation ensemble, and the results will also be reported in the near future in the context of further development of the ensemble data assimilations and the Korean air quality prediction system.

*Code and data availability.* The WRF model v3.8.1 (DOI: <https://doi.org/10.5065/D6MK6B4K>, WRF Users Page, 2022) is available after user registration through the web page ([https://www2.mmm.ucar.edu/wrf/users/download/get\\_source.html](https://www2.mmm.ucar.edu/wrf/users/download/get_source.html), last access: 22 March 2022). The CMAQ model v5.1 (DOI: <https://doi.org/10.5281/zenodo.1079909>, US EPA Office of Research and Development, 2015) is open-source and can be downloaded at <https://github.com/USEPA/CMAQ> (last access: 22 March 2022). The EnKF method and related processes written in IDL language are

available at <https://doi.org/10.5281/zenodo.5376214> (Park, 2021a). We uploaded the model outputs for the ensemble mean with the NetCDF binary format and all the assimilated observation data at <https://doi.org/10.5281/zenodo.5566441> (Park, 2021b).

*Supplement.* The supplement related to this article is available online at: <https://doi.org/10.5194/gmd-15-2773-2022-supplement>.

*Author contributions.* SYP and CHS designed this study and experiments. SYP, UKD, KY, and IU developed the EnKF code and discussed the results. SYP and UKD carried out the simulations, produced the figures, and prepared the initial paper draft. JY performed the 3D-Var experiments and provided all the input data for the CMAQ model. CHS contributed to the final writing with comments from all co-authors.

*Competing interests.* The contact author has declared that neither they nor their co-authors have any competing interests.

*Disclaimer.* Publisher's note: Copernicus Publications remains neutral with regard to jurisdictional claims in published maps and institutional affiliations.

*Acknowledgements.* This research was supported by the FRIEND (Fine Particle Research Initiative in East Asia Considering National Differences) project (2020M3G1A1114617) and Basic Science Research Program (2021R1A2C1006660) of the National Research Foundation of Korea (NRF) with a grant funded by the Ministry of Science and ICT (MSIT). We also appreciate the comments of the reviewers that helped us to improve this article.

*Financial support.* This research has been supported by the National Research Foundation of Korea (grant nos. 2020M3G1A1114617 and 2021R1A2C1006660).

*Review statement.* This paper was edited by Havala Pye and reviewed by two anonymous referees.

## References

- Anderson, J. L.: An Ensemble Adjustment Kalman Filter for Data Assimilation, *Mon. Weather Rev.*, 129, 2884–2903, [https://doi.org/10.1175/1520-0493\(2001\)129<2884:AEAKFF>2.0.CO;2](https://doi.org/10.1175/1520-0493(2001)129<2884:AEAKFF>2.0.CO;2), 2001.
- Appel, K. W., Pouliot, G. A., Simon, H., Sarwar, G., Pye, H. O. T., Napelenok, S. L., Akhtar, F., and Roselle, S. J.: Evaluation of dust and trace metal estimates from the Community Multiscale Air Quality (CMAQ) model version 5.0, *Geosci. Model Dev.*, 6, 883–899, <https://doi.org/10.5194/gmd-6-883-2013>, 2013.
- Benedetti, A., Di Giuseppe, F., Jones, L., Peuch, V.-H., Rémy, S., and Zhang, X.: The value of satellite observations in the analysis and short-range prediction of Asian dust, *Atmos. Chem. Phys.*, 19, 987–998, <https://doi.org/10.5194/acp-19-987-2019>, 2019.
- Bocquet, M., Elbern, H., Eskes, H., Hirtl, M., Žabkar, R., Carmichael, G. R., Flemming, J., Inness, A., Pagowski, M., Pérez Camañó, J. L., Saide, P. E., San Jose, R., Sofiev, M., Vira, J., Baklanov, A., Carnevale, C., Grell, G., and Seigneur, C.: Data assimilation in atmospheric chemistry models: current status and future prospects for coupled chemistry meteorology models, *Atmos. Chem. Phys.*, 15, 5325–5358, <https://doi.org/10.5194/acp-15-5325-2015>, 2015.
- Byun, D. and Schere, K. L.: Review of the Governing Equations, Computational Algorithms, and Other Components of the Models-3 Community Multiscale Air Quality (CMAQ) Modeling System, *Appl. Mech. Rev.*, 59, 51–77, <https://doi.org/10.1115/1.2128636>, 2006.
- Byun, D. W. and Ching, J. K. S.: Science algorithms of the EPA models-3 community multiscale air quality (CMAQ) modeling system, U.S. Environmental Protection Agency, EPA/600/R-99/030 (NTIS PB2000-100561), 1999.
- Candiani, G., Carnevale, C., Finzi, G., Pisoni, E., and Volta, M.: A comparison of reanalysis techniques: Applying optimal interpolation and Ensemble Kalman Filtering to improve air quality monitoring at mesoscale, *Sci. Total Environ.*, 458–460, 7–14, <https://doi.org/10.1016/j.scitotenv.2013.03.089>, 2013.
- Carmichael, G. R., Sakurai, T., Streets, D., Hozumi, Y., Ueda, H., Park, S. U., Fung, C., Han, Z., Kajino, M., Engardt, M., Bennet, C., Hayami, H., Sartelet, K., Holloway, T., Wang, Z., Kannari, A., Fu, J., Matsuda, K., Thongboonchoo, N., and Amann, M.: MICS-Asia II: The model intercomparison study for Asia Phase II methodology and overview of findings, *Atmos. Environ.*, 42, 3468–3490, <https://doi.org/10.1016/j.atmosenv.2007.04.007>, 2008.
- Chai, T., Kim, H.-C., Pan, L., Lee, P., and Tong, D.: Impact of Moderate Resolution Imaging Spectroradiometer Aerosol Optical Depth and AirNow PM<sub>2.5</sub> assimilation on Community Multi-scale Air Quality aerosol predictions over the contiguous United States, *J. Geophys. Res.-Atmos.*, 122, 5399–5415, <https://doi.org/10.1002/2016JD026295>, 2017.
- Chang, L.-S., Cho, A., Park, H., Nam, K., Kim, D., Hong, J.-H., and Song, C.-K.: Human-model hybrid Korean air quality forecasting system, *J. Air Waste Manage.*, 66, 896–911, <https://doi.org/10.1080/10962247.2016.1206995>, 2016.
- Chen, D., Liu, Z., Ban, J., Zhao, P., and Chen, M.: Retrospective analysis of 2015–2017 wintertime PM<sub>2.5</sub> in China: response to emission regulations and the role of meteorology, *Atmos. Chem. Phys.*, 19, 7409–7427, <https://doi.org/10.5194/acp-19-7409-2019>, 2019.
- Cohen, A. J., Brauer, M., Burnett, R., Anderson, H. R., Frostad, J., Estep, K., Balakrishnan, K., Brunekreef, B., Dandona, L., Dandona, R., Feigin, V., Freedman, G., Hubbell, B., Jobling, A., Kan, H., Knibbs, L., Liu, Y., Martin, R., Morawska, L., Pope, C. A., Shin, H., Straif, K., Shaddick, G., Thomas, M., van Dingenen, R., van Donkelaar, A., Vos, T., Murray, C. J. L., and Forouzanfar, M. H.: Estimates and 25-year trends of the global burden of disease attributable to ambient air pollution: an analysis of data from the Global Burden of Diseases Study 2015, *The Lancet*, 389, 1907–1918, [https://doi.org/10.1016/S0140-6736\(17\)30505-6](https://doi.org/10.1016/S0140-6736(17)30505-6), 2017.

- Colella, P. and Woodward, P. R.: The Piecewise Parabolic Method (PPM) for gas-dynamical simulations, *J. Comput. Phys.*, 54, 174–201, [https://doi.org/10.1016/0021-9991\(84\)90143-8](https://doi.org/10.1016/0021-9991(84)90143-8), 1984.
- Coman, A., Foret, G., Beekmann, M., Eremenko, M., Dufour, G., Gaubert, B., Ung, A., Schmechtig, C., Flaud, J.-M., and Bergametti, G.: Assimilation of IASI partial tropospheric columns with an Ensemble Kalman Filter over Europe, *Atmos. Chem. Phys.*, 12, 2513–2532, <https://doi.org/10.5194/acp-12-2513-2012>, 2012.
- Constantinescu, E. M., Sandu, A., Chai, T., and Carmichael, G. R.: Assessment of ensemble-based chemical data assimilation in an idealized setting, *Atmos. Environ.*, 41, 18–36, <https://doi.org/10.1016/j.atmosenv.2006.08.006>, 2007a.
- Constantinescu, E. M., Sandu, A., Chai, T., and Carmichael, G. R.: Ensemble-based chemical data assimilation. II: Covariance localization, *Q. J. Roy. Meteor. Soc.*, 133, 1245–1256, <https://doi.org/10.1002/qj.77>, 2007b.
- Courtier, P., Thépaut, J. N., and Hollingsworth, A.: A strategy for operational implementation of 4D-Var, using an incremental approach, *Q. J. Roy. Meteor. Soc.*, 120, 1367–1387, <https://doi.org/10.1002/qj.49712051912>, 1994.
- Dai, T., Schutgens, N. A. J., Goto, D., Shi, G., and Nakajima, T.: Improvement of aerosol optical properties modeling over Eastern Asia with MODIS AOD assimilation in a global non-hydrostatic icosahedral aerosol transport model, *Environ. Pollut.*, 195, 319–329, <https://doi.org/10.1016/j.envpol.2014.06.021>, 2014.
- Dehghani, M., Keshitgar, L., Javaheri, M. R., Derakhshan, Z., Oliveri Conti, G., Zuccarello, P., and Ferrante, M.: The effects of air pollutants on the mortality rate of lung cancer and leukemia, *Mol. Med. Rep.*, 15, 3390–3397, <https://doi.org/10.3892/mmr.2017.6387>, 2017.
- Eder, B., Kang, D., Mathur, R., Yu, S., and Schere, K.: An operational evaluation of the Eta–CMAQ air quality forecast model, *Atmos. Environ.*, 40, 4894–4905, <https://doi.org/10.1016/j.atmosenv.2005.12.062>, 2006.
- Elbern, H. and Schmidt, H.: Ozone episode analysis by four-dimensional variational chemistry data assimilation, *J. Geophys. Res.-Atmos.*, 106, 3569–3590, <https://doi.org/10.1029/2000JD900448>, 2001.
- Elbern, H., Strunk, A., Schmidt, H., and Talagrand, O.: Emission rate and chemical state estimation by 4-dimensional variational inversion, *Atmos. Chem. Phys.*, 7, 3749–3769, <https://doi.org/10.5194/acp-7-3749-2007>, 2007.
- Evensen, G.: Sequential data assimilation with a nonlinear quasi-geostrophic model using Monte Carlo methods to forecast error statistics, *J. Geophys. Res.-Oceans*, 99, 10143–10162, <https://doi.org/10.1029/94JC00572>, 1994.
- Evensen, G.: The Ensemble Kalman Filter: theoretical formulation and practical implementation, *Ocean Dynam.*, 53, 343–367, <https://doi.org/10.1007/s10236-003-0036-9>, 2003.
- Friedl, M. A., Sulla-Menashe, D., Tan, B., Schneider, A., Ramankutty, N., Sibley, A., and Huang, X.: MODIS Collection 5 global land cover: Algorithm refinements and characterization of new datasets, *Remote Sens. Environ.*, 114, 168–182, <https://doi.org/10.1016/j.rse.2009.08.016>, 2010.
- Gaspari, G. and Cohn, S. E.: Construction of correlation functions in two and three dimensions, *Q. J. Roy. Meteor. Soc.*, 125, 723–757, <https://doi.org/10.1002/qj.49712555417>, 1999.
- Grell, G. A. and Freitas, S. R.: A scale and aerosol aware stochastic convective parameterization for weather and air quality modeling, *Atmos. Chem. Phys.*, 14, 5233–5250, <https://doi.org/10.5194/acp-14-5233-2014>, 2014.
- Guenther, A., Karl, T., Harley, P., Wiedinmyer, C., Palmer, P. I., and Geron, C.: Estimates of global terrestrial isoprene emissions using MEGAN (Model of Emissions of Gases and Aerosols from Nature), *Atmos. Chem. Phys.*, 6, 3181–3210, <https://doi.org/10.5194/acp-6-3181-2006>, 2006.
- Guenther, A. B., Jiang, X., Heald, C. L., Sakulyanontvittaya, T., Duhl, T., Emmons, L. K., and Wang, X.: The Model of Emissions of Gases and Aerosols from Nature version 2.1 (MEGAN2.1): an extended and updated framework for modeling biogenic emissions, *Geosci. Model Dev.*, 5, 1471–1492, <https://doi.org/10.5194/gmd-5-1471-2012>, 2012.
- Ha, S., Liu, Z., Sun, W., Lee, Y., and Chang, L.: Improving air quality forecasting with the assimilation of GOCI aerosol optical depth (AOD) retrievals during the KORUS-AQ period, *Atmos. Chem. Phys.*, 20, 6015–6036, <https://doi.org/10.5194/acp-20-6015-2020>, 2020.
- Hertel, O., Berkowicz, R., Christensen, J., and Hov, Ø.: Test of two numerical schemes for use in atmospheric transport-chemistry models, *Atmos. Environ. A.-Gen.*, 27, 2591–2611, [https://doi.org/10.1016/0960-1686\(93\)90032-T](https://doi.org/10.1016/0960-1686(93)90032-T), 1993.
- Hong, S.-Y.: A new stable boundary-layer mixing scheme and its impact on the simulated East Asian summer monsoon, *Q. J. Roy. Meteor. Soc.*, 136, 1481–1496, <https://doi.org/10.1002/qj.665>, 2010.
- Hong, S.-Y. and Lim, J.-O. J.: The WRF Single-Moment 6-Class Microphysics Scheme (WSM6), *Asia-Pac. J. Atmos. Sci.*, 42, 129–151, 2006.
- Hong, S.-Y., Noh, Y., and Dudhia, J.: A New Vertical Diffusion Package with an Explicit Treatment of Entrainment Processes, *Mon. Weather Rev.*, 134, 2318–2341, <https://doi.org/10.1175/MWR3199.1>, 2006.
- Houtekamer, P. L. and Mitchell, H. L.: Data Assimilation Using an Ensemble Kalman Filter Technique, *Mon. Weather Rev.*, 126, 3, 796–811, [https://doi.org/10.1175/1520-0493\(1998\)126<0796:DAUAEK>2.0.CO;2](https://doi.org/10.1175/1520-0493(1998)126<0796:DAUAEK>2.0.CO;2), 1998.
- Hunt, B. R., Kostelich, E. J., and Szunyogh, I.: Efficient data assimilation for spatiotemporal chaos: A local ensemble transform Kalman filter, *Physica D*, 230, 112–126, <https://doi.org/10.1016/j.physd.2006.11.008>, 2007.
- Hutzell, W. T., Luecken, D. J., Appel, K. W., and Carter, W. P. L.: Interpreting predictions from the SAPRC07 mechanism based on regional and continental simulations, *Atmos. Environ.*, 46, 417–429, <https://doi.org/10.1016/j.atmosenv.2011.09.030>, 2012.
- Iacono, M. J., Delamere, J. S., Mlawer, E. J., Shephard, M. W., Clough, S. A., and Collins, W. D.: Radiative forcing by long-lived greenhouse gases: Calculations with the AER radiative transfer models, *J. Geophys. Res.-Atmos.*, 113, D13103, <https://doi.org/10.1029/2008JD009944>, 2008.
- Jang, Y., Lee, Y., Kim, J., Kim, Y., and Woo, J.-H.: Improvement China Point Source for Improving Bottom-Up Emission Inventory, *Asia-Pac. J. Atmos. Sci.*, 56, 107–118, <https://doi.org/10.1007/s13143-019-00115-y>, 2020.
- Jiang, Z., Liu, Z., Wang, T., Schwartz, C. S., Lin, H.-C., and Jiang, F.: Probing into the impact of 3DVAR assimilation of surface PM<sub>10</sub> observations over China using pro-

- cess analysis, *J. Geophys. Res.-Atmos.*, 118, 6738–6749, <https://doi.org/10.1002/jgrd.50495>, 2013.
- Jiménez, P. A., Dudhia, J., González-Rouco, J. F., Navarro, J., Montávez, J. P., and García-Bustamante, E.: A Revised Scheme for the WRF Surface Layer Formulation, *Mon. Weather Rev.*, 140, 898–918, <https://doi.org/10.1175/MWR-D-11-00056.1>, 2012.
- Jordan, C. E., Crawford, J. H., Beyersdorf, A. J., Eck, T. F., Halliday, H. S., Nault, B. A., Chang, L.-S., Park, J., Park, R., Lee, G., Kim, H., Ahn, J.-y., Cho, S., Shin, H. J., Lee, J. H., Jung, J., Kim, D.-S., Lee, M., Lee, T., Whitehill, A., Szykman, J., Schueneman, M. K., Campuzano-Jost, P., Jimenez, J. L., DiGangi, J. P., Diskin, G. S., Anderson, B. E., Moore, R. H., Ziemba, L. D., Fenn, M. A., Hair, J. W., Kuehn, R. E., Holz, R. E., Chen, G., Travis, K., Shook, M., Peterson, D. A., Lamb, K. D., and Schwarz, J. P.: Investigation of factors controlling PM<sub>2.5</sub> variability across the South Korean Peninsula during KORUS-AQ, *Elementa: Science of the Anthropocene*, 8, 28, <https://doi.org/10.1525/elementa.424>, 2020.
- Kalman, R. E.: A New Approach to Linear Filtering and Prediction Problems, *Journal of Basic Engineering*, 82, 35–45, <https://doi.org/10.1115/1.3662552>, 1960.
- Kalnay, E.: *Atmospheric Modeling, Data Assimilation and Predictability*, Cambridge University Press, Cambridge, <https://doi.org/10.1017/CBO9780511802270>, 2002.
- Lee, E.-H., Ha, J.-C., Lee, S.-S., and Chun, Y.: PM<sub>10</sub> data assimilation over south Korea to Asian dust forecasting model with the optimal interpolation method, *Asia-Pac. J. Atmos. Sci.*, 49, 73–85, <https://doi.org/10.1007/s13143-013-0009-y>, 2013.
- Lee, K., Yu, J., Lee, S., Park, M., Hong, H., Park, S. Y., Choi, M., Kim, J., Kim, Y., Woo, J.-H., Kim, S.-W., and Song, C. H.: Development of Korean Air Quality Prediction System version 1 (KAQPS v1) with focuses on practical issues, *Geosci. Model Dev.*, 13, 1055–1073, <https://doi.org/10.5194/gmd-13-1055-2020>, 2020.
- Lee, S., Song, C. H., Han, K. M., Henze, D. K., Lee, K., Yu, J., Woo, J. H., Jung, J., Choi, Y., Saide, P. E., and Carmichael, G. R.: Impacts of uncertainties in emissions on aerosol data assimilation and short-term PM<sub>2.5</sub> predictions over Northeast Asia, *Atmos. Environ.*, 271, 11921, <https://doi.org/10.1016/j.atmosenv.2021.118921>, 2022.
- Li, Z., Zang, Z., Li, Q. B., Chao, Y., Chen, D., Ye, Z., Liu, Y., and Liou, K. N.: A three-dimensional variational data assimilation system for multiple aerosol species with WRF/Chem and an application to PM<sub>2.5</sub> prediction, *Atmos. Chem. Phys.*, 13, 4265–4278, <https://doi.org/10.5194/acp-13-4265-2013>, 2013.
- Lin, C., Wang, Z., and Zhu, J.: An Ensemble Kalman Filter for severe dust storm data assimilation over China, *Atmos. Chem. Phys.*, 8, 2975–2983, <https://doi.org/10.5194/acp-8-2975-2008>, 2008.
- Liu, Z., Liu, Q., Lin, H.-C., Schwartz, C. S., Lee, Y.-H., and Wang, T.: Three-dimensional variational assimilation of MODIS aerosol optical depth: Implementation and application to a dust storm over East Asia, *J. Geophys. Res.-Atmos.*, 116, D23206, <https://doi.org/10.1029/2011JD016159>, 2011.
- Lopez-Restrepo, S., Yarce, A., Pinel, N., Quintero, O. L., Segers, A., and Heemink, A. W.: Forecasting PM<sub>10</sub> and PM<sub>2.5</sub> in the Aburrá Valley (Medellín, Colombia) via EnKF based data assimilation, *Atmos. Environ.*, 232, 117507, <https://doi.org/10.1016/j.atmosenv.2020.117507>, 2020.
- Lorenc, A. C.: A Global Three-Dimensional Multivariate Statistical Interpolation Scheme, *Mon. Weather Rev.*, 109, 701–721, [https://doi.org/10.1175/1520-0493\(1981\)109<0701:AGTDMS>2.0.CO;2](https://doi.org/10.1175/1520-0493(1981)109<0701:AGTDMS>2.0.CO;2), 1981.
- Lorenc, A. C.: Analysis methods for numerical weather prediction, *Q. J. Roy. Meteor. Soc.*, 112, 1177–1194, <https://doi.org/10.1002/qj.49711247414>, 1986.
- Louis, J.-F.: A parametric model of vertical eddy fluxes in the atmosphere, *Bound.-Lay. Meteorol.*, 17, 187–202, <https://doi.org/10.1007/BF00117978>, 1979.
- Menut, L. and Bessagnet, B.: What Can We Expect from Data Assimilation for Air Quality Forecast? Part I: Quantification with Academic Test Cases, *J. Atmos. Ocean. Tech.*, 36, 269–279, <https://doi.org/10.1175/JTECH-D-18-0002.1>, 2019.
- Morcrette, J. J., Boucher, O., Jones, L., Salmond, D., Bechtold, P., Beljaars, A., Benedetti, A., Bonet, A., Kaiser, J. W., Razinger, M., Schulz, M., Serrar, S., Simmons, A. J., Sofiev, M., Suttie, M., Tompkins, A. M., and Untch, A.: Aerosol analysis and forecast in the European Centre for Medium-Range Weather Forecasts Integrated Forecast System: Forward modeling, *J. Geophys. Res.-Atmos.*, 114, D06206, <https://doi.org/10.1029/2008JD011235>, 2009.
- Myneni, R. B., Hoffman, S., Knyazikhin, Y., Privette, J. L., Glassy, J., Tian, Y., Wang, Y., Song, X., Zhang, Y., Smith, G. R., Lotsch, A., Friedl, M., Morisette, J. T., Votava, P., Nemani, R. R., and Running, S. W.: Global products of vegetation leaf area and fraction absorbed PAR from year one of MODIS data, *Remote Sens. Environ.*, 83, 214–231, [https://doi.org/10.1016/S0034-4257\(02\)00074-3](https://doi.org/10.1016/S0034-4257(02)00074-3), 2002.
- Niu, G.-Y., Yang, Z.-L., Mitchell, K. E., Chen, F., Ek, M. B., Barlage, M., Kumar, A., Manning, K., Niyogi, D., Rosero, E., Tewari, M., and Xia, Y.: The community Noah land surface model with multiparameterization options (Noah-MP): 1. Model description and evaluation with local-scale measurements, *J. Geophys. Res.-Atmos.*, 116, D12109, <https://doi.org/10.1029/2010JD015139>, 2011.
- Otte, T. L. and Pleim, J. E.: The Meteorology-Chemistry Interface Processor (MCIP) for the CMAQ modeling system: updates through MCIPv3.4.1, *Geosci. Model Dev.*, 3, 243–256, <https://doi.org/10.5194/gmd-3-243-2010>, 2010.
- Pagowski, M. and Grell, G. A.: Experiments with the assimilation of fine aerosols using an ensemble Kalman filter, *J. Geophys. Res.-Atmos.*, 117, D21302, <https://doi.org/10.1029/2012JD018333>, 2012.
- Pagowski, M., Grell, G. A., McKeen, S. A., Peckham, S. E., and Devenyi, D.: Three-dimensional variational data assimilation of ozone and fine particulate matter observations: some results using the Weather Research and Forecasting – Chemistry model and Grid-point Statistical Interpolation, *Q. J. Roy. Meteor. Soc.*, 136, 2013–2024, <https://doi.org/10.1002/qj.700>, 2010.
- Pang, J., Liu, Z., Wang, X., Bresch, J., Ban, J., Chen, D., and Kim, J.: Assimilating AOD retrievals from GOCI and VIIRS to forecast surface PM<sub>2.5</sub> episodes over Eastern China, *Atmos. Environ.*, 179, 288–304, <https://doi.org/10.1016/j.atmosenv.2018.02.011>, 2018.
- Park, M. E., Song, C. H., Park, R. S., Lee, J., Kim, J., Lee, S., Woo, J.-H., Carmichael, G. R., Eck, T. F., Holben, B. N., Lee, S.-S., Song, C. K., and Hong, Y. D.: New approach to monitor transboundary particulate pollution over Northeast Asia, *Atmos.*



- Chem. Phys., 14, 659–674, <https://doi.org/10.5194/acp-14-659-2014>, 2014.
- Park, R. S., Song, C. H., Han, K. M., Park, M. E., Lee, S.-S., Kim, S.-B., and Shimizu, A.: A study on the aerosol optical properties over East Asia using a combination of CMAQ-simulated aerosol optical properties and remote-sensing data via a data assimilation technique, *Atmos. Chem. Phys.*, 11, 12275–12296, <https://doi.org/10.5194/acp-11-12275-2011>, 2011.
- Park, S.-Y.: Implementation of an Ensemble Kalman Filter in the Community Multiscale Air Quality Model (CMAQ Model v5.1) for Data Assimilation of Ground-level PM<sub>2.5</sub>: Data Assimilation Codes, Zenodo [code], <https://doi.org/10.5281/zenodo.5376214>, 2021a.
- Park, S.-Y.: Implementation of an Ensemble Kalman Filter in the Community Multiscale Air Quality Model (CMAQ Model v5.1) for Data Assimilation of Ground-level PM<sub>2.5</sub>: Model Simulation Outputs, Zenodo [data set], <https://doi.org/10.5281/zenodo.5566441>, 2021b.
- Park, S.-Y., Kim, D.-H., Lee, S.-H., and Lee, H. W.: Variational data assimilation for the optimized ozone initial state and the short-time forecasting, *Atmos. Chem. Phys.*, 16, 3631–3649, <https://doi.org/10.5194/acp-16-3631-2016>, 2016.
- Parrish, D. F. and Derber, J. C.: The National Meteorological Center's Spectral Statistical-Interpolation Analysis System, *Mon. Weather Rev.*, 120, 1747–1763, [https://doi.org/10.1175/1520-0493\(1992\)120<1747:TNMCS>2.0.CO;2](https://doi.org/10.1175/1520-0493(1992)120<1747:TNMCS>2.0.CO;2), 1992.
- Peng, Z., Liu, Z., Chen, D., and Ban, J.: Improving PM<sub>2.5</sub> forecast over China by the joint adjustment of initial conditions and source emissions with an ensemble Kalman filter, *Atmos. Chem. Phys.*, 17, 4837–4855, <https://doi.org/10.5194/acp-17-4837-2017>, 2017.
- Peng, Z., Lei, L., Liu, Z., Sun, J., Ding, A., Ban, J., Chen, D., Kou, X., and Chu, K.: The impact of multi-species surface chemical observation assimilation on air quality forecasts in China, *Atmos. Chem. Phys.*, 18, 17387–17404, <https://doi.org/10.5194/acp-18-17387-2018>, 2018.
- Peterson, D. A., Hyer, E. J., Han, S.-O., Crawford, J. H., Park, R. J., Holz, R., Kuehn, R. E., Eloranta, E., Knote, C., Jordan, C. E., and Lefer, B. L.: Meteorology influencing springtime air quality, pollution transport, and visibility in Korea, *Elementa: Science of the Anthropocene*, 7, 57, <https://doi.org/10.1525/elementa.395>, 2019.
- Pleim, J. E.: A Combined Local and Nonlocal Closure Model for the Atmospheric Boundary Layer. Part I: Model Description and Testing, *J. Appl. Meteorol. Clim.*, 46, 1383–1395, <https://doi.org/10.1175/JAM2539.1>, 2007a.
- Pleim, J. E.: A Combined Local and Nonlocal Closure Model for the Atmospheric Boundary Layer. Part II: Application and Evaluation in a Mesoscale Meteorological Model, *J. Appl. Meteorol. Clim.*, 46, 1396–1409, <https://doi.org/10.1175/JAM2534.1>, 2007b.
- Pleim, J. E. and Xiu, A.: Development of a Land Surface Model. Part II: Data Assimilation, *J. Appl. Meteorol.*, 42, 1811–1822, [https://doi.org/10.1175/1520-0450\(2003\)042<1811:DOALSM>2.0.CO;2](https://doi.org/10.1175/1520-0450(2003)042<1811:DOALSM>2.0.CO;2), 2003.
- Pope, C. A. and Dockery, D. W.: Health Effects of Fine Particulate Air Pollution: Lines that Connect, *J. Air Waste Manage.*, 56, 709–742, <https://doi.org/10.1080/10473289.2006.10464485>, 2006.
- Rabier, F., McNally, A., Andersson, E., Courtier, P., Undén, P., Eyre, J., Hollingsworth, A., and Bouttier, F.: The ECMWF implementation of three-dimensional variational assimilation (3D-Var). II: Structure functions, *Q. J. Roy. Meteor. Soc.*, 124, 1809–1829, <https://doi.org/10.1002/qj.49712455003>, 1998.
- Rabier, F., Järvinen, H., Klinker, E., Mahfouf, J. F., and Simmons, A.: The ECMWF operational implementation of four-dimensional variational assimilation. I: Experimental results with simplified physics, *Q. J. Roy. Meteor. Soc.*, 126, 1143–1170, <https://doi.org/10.1002/qj.49712656415>, 2000.
- Roustan, Y. and Bocquet, M.: Inverse modelling for mercury over Europe, *Atmos. Chem. Phys.*, 6, 3085–3098, <https://doi.org/10.5194/acp-6-3085-2006>, 2006.
- Rubin, J. I., Reid, J. S., Hansen, J. A., Anderson, J. L., Collins, N., Hoar, T. J., Hogan, T., Lynch, P., McLay, J., Reynolds, C. A., Sessions, W. R., Westphal, D. L., and Zhang, J.: Development of the Ensemble Navy Aerosol Analysis Prediction System (ENAAAPS) and its application of the Data Assimilation Research Testbed (DART) in support of aerosol forecasting, *Atmos. Chem. Phys.*, 16, 3927–3951, <https://doi.org/10.5194/acp-16-3927-2016>, 2016.
- Saha, S., Moorthi, S., Pan, H.-L., Wu, X., Wang, J., Nadiga, S., Tripp, P., Kistler, R., Woollen, J., Behringer, D., Liu, H., Stokes, D., Grumbine, R., Gayno, G., Wang, J., Hou, Y.-T., Chuang, H.-Y., Juang, H.-M. H., Sela, J., Iredell, M., Treadon, R., Kleist, D., Van Delst, P., Keyser, D., Derber, J., Ek, M., Meng, J., Wei, H., Yang, R., Lord, S., van den Dool, H., Kumar, A., Wang, W., Long, C., Chelliah, M., Xue, Y., Huang, B., Schemm, J.-K., Ebisuzaki, W., Lin, R., Xie, P., Chen, M., Zhou, S., Higgins, W., Zou, C.-Z., Liu, Q., Chen, Y., Han, Y., Cucurull, L., Reynolds, R. W., Rutledge, G., and Goldberg, M.: NCEP Climate Forecast System Reanalysis (CFSR) 6-hourly Products, January 1979 to December 2010, Research Data Archive at the National Center for Atmospheric Research, Computational and Information Systems Laboratory [data set], <https://doi.org/10.5065/D69K487J>, 2010.
- Saide, P. E., Carmichael, G. R., Liu, Z., Schwartz, C. S., Lin, H. C., da Silva, A. M., and Hyer, E.: Aerosol optical depth assimilation for a size-resolved sectional model: impacts of observationally constrained, multi-wavelength and fine mode retrievals on regional scale analyses and forecasts, *Atmos. Chem. Phys.*, 13, 10425–10444, <https://doi.org/10.5194/acp-13-10425-2013>, 2013.
- Sandu, A. and Chai, T.: Chemical Data Assimilation – An Overview, *Atmosphere*, 2, 426–463, <https://doi.org/10.3390/atmos2030426>, 2011.
- Schutgens, N. A. J., Miyoshi, T., Takemura, T., and Nakajima, T.: Applying an ensemble Kalman filter to the assimilation of AERONET observations in a global aerosol transport model, *Atmos. Chem. Phys.*, 10, 2561–2576, <https://doi.org/10.5194/acp-10-2561-2010>, 2010.
- Schwartz, C. S., Liu, Z., Lin, H.-C., and McKeen, S. A.: Simultaneous three-dimensional variational assimilation of surface fine particulate matter and MODIS aerosol optical depth, *J. Geophys. Res.-Atmos.*, 117, D13202, <https://doi.org/10.1029/2011JD017383>, 2012.
- Schwartz, C. S., Liu, Z., Lin, H.-C., and Cetola, J. D.: Assimilating aerosol observations with a “hybrid” variational-ensemble data

- assimilation system, *J. Geophys. Res.-Atmos.*, 119, 4043–4069, <https://doi.org/10.1002/2013JD020937>, 2014.
- Sekiyama, T. T., Tanaka, T. Y., Shimizu, A., and Miyoshi, T.: Data assimilation of CALIPSO aerosol observations, *Atmos. Chem. Phys.*, 10, 39–49, <https://doi.org/10.5194/acp-10-39-2010>, 2010.
- Shao, H., Derber, J., Huang, X.-Y., Hu, M., Newman, K., Stark, D., Lueken, M., Zhou, C., Nance, L., Kuo, Y.-H., and Brown, B.: Bridging Research to Operations Transitions: Status and Plans of Community GSI, *B. Am. Meteorol. Soc.*, 97, 1427–1440, <https://doi.org/10.1175/BAMS-D-13-00245.1>, 2016.
- Skachko, S., Errera, Q., Ménard, R., Christophe, Y., and Chabrilat, S.: Comparison of the ensemble Kalman filter and 4D-Var assimilation methods using a stratospheric tracer transport model, *Geosci. Model Dev.*, 7, 1451–1465, <https://doi.org/10.5194/gmd-7-1451-2014>, 2014.
- Skamarock, W. C., Klemp, J. B., Dudhia, J., Gill, D. O., Barker, D., Duda, M. G., Huang, X., Wang, W., and Powers, J. G.: A Description of the Advanced Research WRF Version 3, University Corporation for Atmospheric Research, no. NCAR/TN-475+STR, <https://doi.org/10.5065/D68S4MVH>, 2008.
- Solazzo, E., Bianconi, R., Pirovano, G., Matthias, V., Vautard, R., Moran, M. D., Wyatt Appel, K., Bessagnet, B., Brandt, J., Christensen, J. H., Chemel, C., Coll, I., Ferreira, J., Forkel, R., Francis, X. V., Grell, G., Grossi, P., Hansen, A. B., Miranda, A. I., Nopmongcol, U., Prank, M., Sartelet, K. N., Schaap, M., Silver, J. D., Sokhi, R. S., Vira, J., Werhahn, J., Wolke, R., Yarwood, G., Zhang, J., Rao, S. T., and Galmarini, S.: Operational model evaluation for particulate matter in Europe and North America in the context of AQMEII, *Atmos. Environ.*, 53, 75–92, <https://doi.org/10.1016/j.atmosenv.2012.02.045>, 2012.
- Stauffer, D. R. and Seaman, N. L.: Use of Four-Dimensional Data Assimilation in a Limited-Area Mesoscale Model. Part I: Experiments with Synoptic-Scale Data, *Mon. Weather Rev.*, 118, 1250–1277, [https://doi.org/10.1175/1520-0493\(1990\)118<1250:UOFDDA>2.0.CO;2](https://doi.org/10.1175/1520-0493(1990)118<1250:UOFDDA>2.0.CO;2), 1990.
- Talagrand, O. and Courtier, P.: Variational Assimilation of Meteorological Observations With the Adjoint Vorticity Equation. I: Theory, *Q. J. Roy. Meteor. Soc.*, 113, 1311–1328, <https://doi.org/10.1002/qj.49711347812>, 1987.
- Tang, X., Zhu, J., Wang, Z. F., and Gbaguidi, A.: Improvement of ozone forecast over Beijing based on ensemble Kalman filter with simultaneous adjustment of initial conditions and emissions, *Atmos. Chem. Phys.*, 11, 12901–12916, <https://doi.org/10.5194/acp-11-12901-2011>, 2011.
- Tang, Y., Chai, T., Pan, L., Lee, P., Tong, D., Kim, H.-C., and Chen, W.: Using optimal interpolation to assimilate surface measurements and satellite AOD for ozone and PM<sub>2.5</sub>: A case study for July 2011, *J. Air Waste Manage.*, 65, 1206–1216, <https://doi.org/10.1080/10962247.2015.1062439>, 2015.
- Tang, Y., Pagowski, M., Chai, T., Pan, L., Lee, P., Baker, B., Kumar, R., Delle Monache, L., Tong, D., and Kim, H.-C.: A case study of aerosol data assimilation with the Community Multi-scale Air Quality Model over the contiguous United States using 3D-Var and optimal interpolation methods, *Geosci. Model Dev.*, 10, 4743–4758, <https://doi.org/10.5194/gmd-10-4743-2017>, 2017.
- US EPA Office of Research and Development: CMAQv5.1 (5.1), Zenodo [code], <https://doi.org/10.5281/zenodo.1079909>, 2015.
- Whitaker, J. S. and Hamill, T. M.: Ensemble Data Assimilation without Perturbed Observations, *Mon. Weather Rev.*, 130, 1913–1924, [https://doi.org/10.1175/1520-0493\(2002\)130<1913:EDAWPO>2.0.CO;2](https://doi.org/10.1175/1520-0493(2002)130<1913:EDAWPO>2.0.CO;2), 2002.
- Whitaker, J. S. and Hamill, T. M.: Evaluating Methods to Account for System Errors in Ensemble Data Assimilation, *Mon. Weather Rev.*, 140, 3078–3089, <https://doi.org/10.1175/MWR-D-11-00276.1>, 2012.
- Wiedinmyer, C., Quayle, B., Geron, C., Belote, A., McKenzie, D., Zhang, X., O'Neill, S., and Wynne, K. K.: Estimating emissions from fires in North America for air quality modeling, *Atmos. Environ.*, 40, 3419–3432, <https://doi.org/10.1016/j.atmosenv.2006.02.010>, 2006.
- Wiedinmyer, C., Akagi, S. K., Yokelson, R. J., Emmons, L. K., Al-Saadi, J. A., Orlando, J. J., and Soja, A. J.: The Fire INventory from NCAR (FINN): a high resolution global model to estimate the emissions from open burning, *Geosci. Model Dev.*, 4, 625–641, <https://doi.org/10.5194/gmd-4-625-2011>, 2011.
- WRF Users Page: WRF Model Users' Page, WRF Users Page [code], <https://doi.org/10.5065/D6MK6B4K>, 2022.
- Yamartino, R. J.: Nonnegative, Conserved Scalar Transport Using Grid-Cell-centered, Spectrally Constrained Blackman Cubics for Applications on a Variable-Thickness Mesh, *Mon. Weather Rev.*, 121, 753–763, [https://doi.org/10.1175/1520-0493\(1993\)121<0753:NCSTUG>2.0.CO;2](https://doi.org/10.1175/1520-0493(1993)121<0753:NCSTUG>2.0.CO;2), 1993.
- Yang, Z.-L., Niu, G.-Y., Mitchell, K. E., Chen, F., Ek, M. B., Barlage, M., Longuevergne, L., Manning, K., Niyogi, D., Tewari, M., and Xia, Y.: The community Noah land surface model with multiparameterization options (Noah-MP): 2. Evaluation over global river basins, *J. Geophys. Res.-Atmos.*, 116, D12110, <https://doi.org/10.1029/2010JD015140>, 2011.
- Yin, X.-M., Dai, T., Xin, J.-Y., Gong, D.-Y., Yang, J., Teruyuki, N., and Shi, G.-Y.: Estimation of aerosol properties over the Chinese desert region with MODIS AOD assimilation in a global model, *Adv. Clim. Chang. Res.*, 7, 90–98, <https://doi.org/10.1016/j.accre.2016.04.001>, 2016.
- Yuan, H., Dai, Y., Xiao, Z., Ji, D., and Shangguan, W.: Reprocessing the MODIS Leaf Area Index products for land surface and climate modelling, *Remote Sens. Environ.*, 115, 1171–1187, <https://doi.org/10.1016/j.rse.2011.01.001>, 2011.
- Yumimoto, K. and Takemura, T.: Long-term inverse modeling of Asian dust: Interannual variations of its emission, transport, deposition, and radiative forcing, *J. Geophys. Res.-Atmos.*, 120, 1582–1607, <https://doi.org/10.1002/2014JD022390>, 2015.
- Yumimoto, K., Nagao, T. M., Kikuchi, M., Sekiyama, T. T., Murakami, H., Tanaka, T. Y., Ogi, A., Irie, H., Khatri, P., Okumura, H., Arai, K., Morino, I., Uchino, O., and Maki, T.: Aerosol data assimilation using data from Himawari-8, a next-generation geostationary meteorological satellite, *Geophys. Res. Lett.*, 43, 5886–5894, <https://doi.org/10.1002/2016GL069298>, 2016.
- Zhang, Y., Bocquet, M., Mallet, V., Seigneur, C., and Baklanov, A.: Real-time air quality forecasting, part II: State of the science, current research needs, and future prospects, *Atmos. Environ.*, 60, 656–676, <https://doi.org/10.1016/j.atmosenv.2012.02.041>, 2012a.
- Zhang, Y., Bocquet, M., Mallet, V., Seigneur, C., and Baklanov, A.: Real-time air quality forecasting, part I: History, techniques, and current status, *Atmos. Environ.*, 60, 632–655, <https://doi.org/10.1016/j.atmosenv.2012.06.031>, 2012b.